Electronic supplementary information

Sustainable gas conversion by gliding arc plasmas: a new modelling approach for reactor design improvement.

Senne Van Alphen,*[1,2], Fatme Jardali[1], James Creel[1], Georgi Trenchev[1], Rony Snyders[2] and Annemie Bogaerts[1]

[1] Research group PLASMANT, Department of Chemistry, University of Antwerp, Universiteitsplein 1, 2610 Antwerp, Belgium.

[2] Research group ChIPS, Department of Chemistry, University of Mons, Av. Nicolas Copernic 3, 7000 Mons, Belgium.

S1. Gas properties of the 3D turbulent flow model and thermal plasma model.

The material properties used in the 3D turbulent flow model and the thermal plasma model are adopted from the COMSOL 5.5 material database for air.[2] The temperature dependencies of these properties are considered by interpolation of the property values listed in table S1. In this table T is the temperature, ρ the gas density, C_p the heat capacity at constant pressure, μ the dynamic viscosity, k the thermal conductivity, and σ the electrical conductivity.

Table S1: Temperature dependency of the properties considered in the 3D turbulent flow model and thermal plasma model.

$T\ (K)$	$\rho\left(\frac{kg}{m^3}\right)$	$C_p\left(\frac{J}{kg\ K}\right)$	$\mu(Pa.s)$	$k\left(\frac{W}{m\ K}\right)$	$\sigma\left(\frac{S}{m}\right)$
500	7.020E-01	1.047E+03	2.710E-05	4.100E-02	0.000
600	5.850E-01	1.069E+03	3.080E-05	4.800E-02	0.000
700	5.010E-01	1.086E+03	3.440E-05	5.500E-02	0.000
800	4.390E-01	1.103E+03	3.790E-05	6.200E-02	0.000
900	3.900E-01	1.119E+03	4.120E-05	6.800E-02	0.000
1000	3.510E-01	1.135E+03	4.450E-05	7.500E-02	0.000
1100	3.190E-01	1.151E+03	4.760E-05	8.100E-02	0.000
1200	2.930E-01	1.167E+03	5.070E-05	8.800E-02	0.000
1300	2.700E-01	1.184E+03	5.370E-05	9.400E-02	0.000
1400	2.510E-01	1.201E+03	5.660E-05	1.010E-01	0.000
1500	2.340E-01	1.219E+03	5.950E-05	1.070E-01	0.000
1600	2.190E-01	1.237E+03	6.240E-05	1.140E-01	0.000
1700	2.070E-01	1.257E+03	6.520E-05	1.210E-01	0.000
1800	1.950E-01	1.278E+03	6.790E-05	1.280E-01	0.000
1900	1.850E-01	1.301E+03	7.060E-05	1.360E-01	0.000
2000	1.760E-01	1.328E+03	7.330E-05	1.450E-01	0.000

2100	1.670E-01	1.361E+03	7.590E-05	1.550E-01	0.000
2200	1.590E-01	1.403E+03	7.860E-05	1.680E-01	0.000
2300	1.520E-01	1.456E+03	8.120E-05	1.830E-01	0.000
2400	1.460E-01	1.527E+03	8.370E-05	2.030E-01	0.000
2500	1.400E-01	1.620E+03	8.630E-05	2.280E-01	0.000
2600	1.340E-01	1.741E+03	8.880E-05	2.600E-01	0.000
2700	1.290E-01	1.894E+03	9.140E-05	3.010E-01	1.000E-03
2800	1.240E-01	2.084E+03	9.390E-05	3.500E-01	2.000E-03
2900	1.190E-01	2.310E+03	9.650E-05	4.070E-01	4.000E-03
3000	1.140E-01	2.569E+03	9.900E-05	4.720E-01	9.000E-03
3100	1.100E-01	2.855E+03	1.017E-04	5.420E-01	3.600E-02
3200	1.050E-01	3.151E+03	1.043E-04	6.100E-01	6.400E-02
3300	1.010E-01	3.435E+03	1.070E-04	6.720E-01	1.100E-01
3400	9.700E-02	3.679E+03	1.097E-04	7.190E-01	1.820E-01
3500	9.300E-02	3.852E+03	1.125E-04	7.460E-01	2.900E-01
3600	8.900E-02	3.927E+03	1.152E-04	7.500E-01	4.440E-01
3700	8.600E-02	3.891E+03	1.179E-04	7.310E-01	6.620E-01
3800	8.200E-02	3.750E+03	1.205E-04	6.930E-01	9.580E-01
3900	7.900E-02	3.528E+03	1.231E-04	6.460E-01	1.351E+00
4000	7.600E-02	3.264E+03	1.257E-04	5.980E-01	1.861E+00
4100	7.400E-02	2.997E+03	1.282E-04	5.550E-01	2.510E+00
4200	7.200E-02	2.758E+03	1.307E-04	5.220E-01	3.325E+00
4300	7.000E-02	2.567E+03	1.331E-04	5.010E-01	4.332E+00
4400	6.800E-02	2.432E+03	1.356E-04	4.930E-01	5.563E+00
4500	6.600E-02	2.353E+03	1.379E-04	4.970E-01	7.051E+00
4600	6.400E-02	2.330E+03	1.403E-04	5.150E-01	8.831E+00
4700	6.300E-02	2.357E+03	1.426E-04	5.440E-01	1.094E+01
4800	6.100E-02	2.433E+03	1.450E-04	5.870E-01	1.343E+01
4900	6.000E-02	2.556E+03	1.473E-04	6.420E-01	1.633E+01
5000	5.800E-02	2.725E+03	1.496E-04	7.110E-01	1.968E+01
5100	5.700E-02	2.940E+03	1.519E-04	7.940E-01	2.355E+01
5200	5.600E-02	3.202E+03	1.543E-04	8.920E-01	2.798E+01
5300	5.400E-02	3.515E+03	1.566E-04	1.006E+00	3.301E+01
5400	5.300E-02	3.818E+03	1.589E-04	1.137E+00	3.871E+01
5500	5.200E-02	4.295E+03	1.612E-04	1.286E+00	4.511E+01
5600	5.000E-02	4.767E+03	1.636E-04	1.452E+00	5.230E+01
5700	4.900E-02	5.295E+03	1.660E-04	1.636E+00	6.035E+01
5800	4.800E-02	5.880E+03	1.683E-04	1.837E+00	6.928E+01
5900	4.600E-02	6.520E+03	1.707E-04	2.053E+00	7.918E+01
6000	4.500E-02	7.212E+03	1.731E-04	2.283E+00	9.019E+01
6100	4.300E-02	7.952E+03	1.755E-04	2.522E+00	1.024E+02
6200	4.200E-02	8.730E+03	1.778E-04	2.767E+00	1.159E+02
6300	4.100E-02	9.534E+03	1.802E-04	3.011E+00	1.309E+02
6400	3.900E-02	1.035E+04	1.825E-04	3.248E+00	1.475E+02
6500	3.800E-02	1.115E+04	1.848E-04	3.471E+00	1.659E+02
6600	3.700E-02	1.192E+04	1.870E-04	3.670E+00	1.865E+02

6700	3.500E-02	1.262E+04	1.892E-04	3.837E+00	2.095E+02
6800	3.400E-02	1.323E+04	1.913E-04	3.963E+00	2.352E+02
6900	3.300E-02	1.371E+04	1.933E-04	4.043E+00	2.641E+02
7000	3.200E-02	1.403E+04	1.952E-04	4.070E+00	2.965E+02
7100	3.000E-02	1.416E+04	1.970E-04	4.043E+00	3.327E+02
7200	2.900E-02	1.411E+04	1.988E-04	3.964E+00	3.731E+02
7300	2.800E-02	1.386E+04	2.005E-04	3.837E+00	4.178E+02
7400	2.700E-02	1.343E+04	2.021E-04	3.670E+00	4.670E+02
7500	2.700E-02	1.284E+04	2.037E-04	3.473E+00	5.208E+02
7600	2.600E-02	1.213E+04	2.053E-04	3.256E+00	5.790E+02
7700	2.500E-02	1.134E+04	2.069E-04	3.031E+00	6.417E+02
7800	2.400E-02	1.051E+04	2.086E-04	2.806E+00	7.085E+02
7900	2.400E-02	9.678E+03	2.102E-04	2.591E+00	7.794E+02
8000	2.300E-02	8.871E+03	2.119E-04	2.390E+00	8.540E+02
8100	2.300E-02	8.113E+03	2.136E-04	2.208E+00	9.321E+02
8200	2.200E-02	7.426E+03	2.153E-04	2.046E+00	1.014E+03
8300	2.200E-02	6.806E+03	2.171E-04	1.907E+00	1.098E+03
8400	2.200E-02	6.268E+03	2.189E-04	1.788E+00	1.185E+03
8500	2.100E-02	5.807E+03	2.207E-04	1.690E+00	1.275E+03
8600	2.100E-02	5.428E+03	2.225E-04	1.611E+00	1.367E+03
8700	2.000E-02	5.103E+03	2.243E-04	1.550E+00	1.462E+03
8800	2.000E-02	4.857E+03	2.261E-04	1.504E+00	1.558E+03
8900	2.000E-02	4.647E+03	2.279E-04	1.471E+00	1.657E+03
9000	2.000E-02	4.497E+03	2.297E-04	1.451E+00	1.756E+03
9100	1.900E-02	4.408E+03	2.315E-04	1.443E+00	1.858E+03
9200	1.900E-02	4.327E+03	2.332E-04	1.443E+00	1.961E+03
9300	1.900E-02	4.318E+03	2.349E-04	1.454E+00	2.064E+03
9400	1.900E-02	4.302E+03	2.366E-04	1.471E+00	2.169E+03
9500	1.800E-02	4.353E+03	2.382E-04	1.497E+00	2.275E+03
9600	1.800E-02	4.418E+03	2.398E-04	1.529E+00	2.382E+03
9700	1.800E-02	4.463E+03	2.413E-04	1.565E+00	2.489E+03
9800	1.800E-02	4.605E+03	2.421E-04	1.609E+00	2.597E+03
9900	1.700E-02	4.689E+03	2.441E-04	1.656E+00	2.706E+03
10000	1.700E-02	4.867E+03	2.453E-04	1.709E+00	2.814E+03

S2. Turbulent flow Shear Stress Tensor model

The turbulent model applied in our study is the RANS (Reynolds-Averaged-Navier-Stokes) SST (Shear Stress Tensor) model, which uses the common k-ε model in the free stream and combines it with the more accurate k-ω model near the walls.[1] In this k-ω model the viscous layer at the boundaries is fully resolved, i.e. the model is more accurate for the flow near the walls than in models where so-called wall functions are used that employ analytical solutions for the behaviour near the walls. This approach includes the following equations for the turbulent kinetic energy k and the specific dissipation ω:

$$\rho(\vec{u_g}.\nabla)k = \nabla\cdot\left[(\mu+\mu_T\sigma_k)\nabla k\right] + P - \beta_0\rho\omega k \ \#(1)$$

$$\rho(\vec{u_g}.\nabla)\omega = \nabla\cdot\left[(\mu+\mu_T\sigma_\omega)\nabla\omega\right] + \frac{\gamma}{\mu_T}\rho P - \beta_0\rho\omega^2 + 2(1-f_{v1})\frac{\sigma_{\omega2}\rho}{\omega}\nabla k\cdot\nabla\omega \ \#(2)$$

Where ρ stands for the gas density, $\vec{u_g}$ is the gas flow velocity vector, μ is the dynamic viscosity, σ_k, σ_ω and γ are model coefficients defined in equation 10, 11 and 12, and β_0 and $\sigma_{\omega2}$ are dimensionless model constants defined in table S1. The other symbols are explained below.

In equation 1 and 2, μ_T is the turbulent viscosity of the fluid and is defined as:

$$\mu_T = \frac{a_1 k}{max(a_1\omega, Sf_{v2})} \ \#(3)$$

In which S is the absolute strain rate and a_1 is a dimensionless model constant defined in table S1.

In equation 2 and 3, f_{v1} and f_{v2} are two blending functions that control the switch from the k-ω model to the k-ε model in the free stream (where f_{v1} = 1)

$$f_{v1} = \tanh\left(\min\left(\theta_2^2, \frac{4\sigma_{\omega2}k}{CD_{k\omega}y^2}\right)\right)^4 \ \#(4)$$

$$f_{v2} = \tanh\left(\theta_2^2\right) \ \#(5)$$

In which y is the y-component of the position vector, and θ_2 and $CD_{k\omega}$ are placeholders for the following terms:

$$CD_{k\omega} = max\left(2\rho\sigma_{\omega2}\frac{1}{\omega}\frac{\partial k}{\partial x}\frac{\partial\omega}{\partial x}, 10^{-10}\right) \ \#(6)$$

$$\theta_2 = max\left(\frac{2\sqrt{k}}{\beta_0\omega l_W^2}, \frac{500\mu}{y^2\omega}\right) \ \#(7)$$

In which l_W is the wall distance.

In equation 1 and 2, P serves as a product limiter coefficient and is defined as:

$$P = \min\left(P_k 10\rho\beta_0 k\omega\right) \ \#(8)$$

In which P_k is a placeholder for the following term:

$$P_k = \mu_T\left(\nabla\vec{u_g}:\left(\nabla\vec{u_g} + \left(\nabla\vec{u_g}\right)^T\right) - \frac{2}{3}\cdot\left(\nabla\cdot\vec{u_g}\right)^2\right) - \frac{2}{3}\rho k\nabla\cdot\vec{u_g}\ \#(9)$$

The model coefficients in equation 1 and 2 are defined as

$$\sigma_k = f_{v1}\cdot\sigma_{k1} + (1 - f_{v1})\sigma_{k2}\#(10)$$

$$\sigma_\omega = f_{v1}\cdot\sigma_{\omega1} + (1 - f_{v1})\sigma_{\omega2}\#(11)$$

$$\gamma = f_{v1}\cdot\gamma_1 + (1 - f_{v1})\gamma_2\#(12)$$

In which σ_{k1}, σ_{k2}, $\sigma_{\omega1}$,$\sigma_{\omega2}$, γ_1 and γ_2 are dimensionless model constants defined in table S2.

Table S2: dimensionless model constants used in the SST turbulent flow model.

σ_{k1}	0.85
σ_{k2}	1
$\sigma_{\omega1}$	0.5
$\sigma_{\omega2}$	0.856
γ_1	0.5556
γ_2	0.44
a_1	0.31
β_0	0.09

S3. Circuit of the 3D thermal plasma model

The scheme in figure S1 represents the electrical circuit of the RGA reactor. The cathode pin is connected to a ballast resistor, which in turn is connected to a voltage source supplying 3 kV, while the anode wall is grounded. The current is limited by a ballast 200 Ω resistor (Rb), and a 10 pF capacitor (Cb) forms an RC filtering circuit. The total current for the system is varied by changing the value for the ballast resistor.

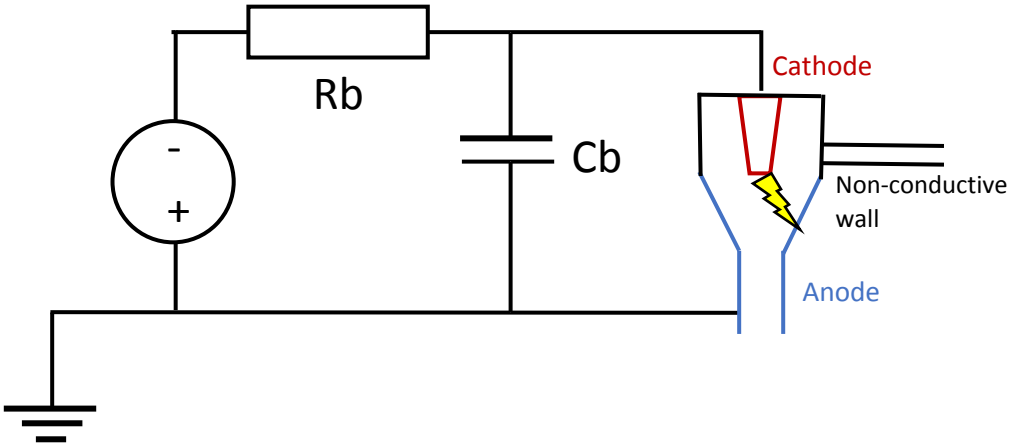

Figure S1: Representative electrical scheme of the RGA reactor.

S4. Scaling of the 3D thermal plasma temperature

The calculated gas temperature of the thermal plasma model is scaled using the results of the axi-symmetric 2D non-thermal plasma model that correctly incorporates the heat terms of all plasma processes and reactions occurring in an N_2/O_2 plasma. As shown by the axi-symmetric temperature profile in figure S2, the maximum temperature in the plasma is around 3500 K.

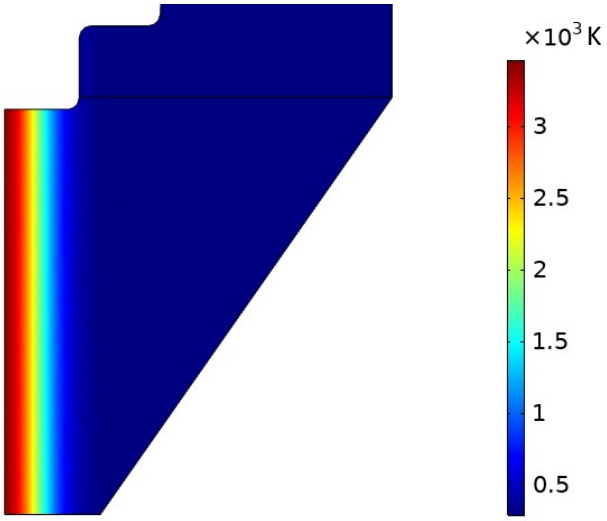

Figure S2: Calculated axi-symmetric temperature profile of the 2D non-thermal plasma model

As the thermal model correctly describes the gas temperature gradients, the absolute values of the temperature are corrected using the following formula:

$$\frac{T - 293.15}{T_{factor}} + 293.15 \ \#(13)$$

Where T is the unscaled gas temperature, calculated by the 3D thermal plasma model and T_{factor} the correction factor to match T to the temperature of the 2D non-thermal plasma model, which was found to be 3.15.

The original (uncorrected) and the corrected temperature profile, resulting from the 3D thermal plasma model, are shown in figure S3.

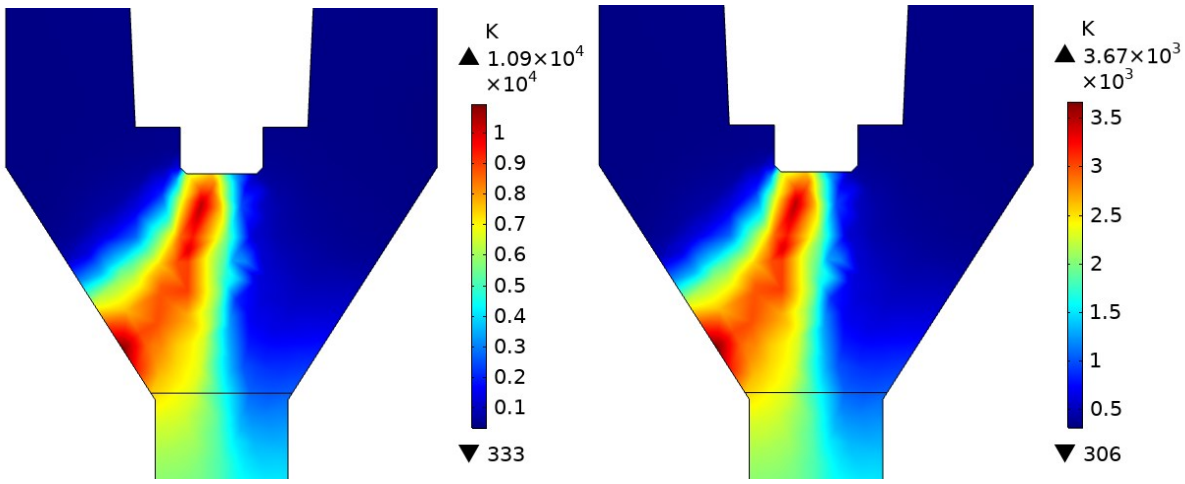

Figure S3: Original (uncorrected) (a) and corrected (b) temperature profiles of the thermal plasma model.

S5. Drag force of the particle tracing simulations

The molecule trajectories in the particle tracing simulations are calculated using the drag force and velocity fields that were previously computed by the turbulent flow model. This drag force F_D is calculated as follows:

$$\vec{F_D} = \frac{1}{\tau_p S} m_p \left(\vec{u_g} - \vec{v_p}\right) \#(14)$$

In which m_p is the mass of the particle, $\vec{u_g}$ the velocity field calculated by the turbulent flow model and $\vec{v_p}$ the particle velocity, which differs from $\vec{u_g}$ due the inertia of the particles.

In equation 14, τ_p and S are calculated using:

$$\tau_p = \frac{\rho_p d_p^2}{18\mu} \#(15)$$

In which ρ_p is the particle density, d_p the particle diameter and μ the dynamic viscosity of the fluid (see above).

$$S = 1 + K_n\left(C_1 + C_2 exp\left(-\frac{C_3}{K_n}\right)\right) \#(16)$$

In which K_n is a placeholder for following term:

$$K_n = \frac{\mu}{d_p}\sqrt{\frac{\pi}{2p\rho}} \#(17)$$

In which ρ and p are the gas density and gas pressure, respectively, as calculated by the turbulent flow model.

In equation 16, C_1, C_2 and C_3 are the Cunningham-Millikan-Davies coefficients that consider rarefaction with the following values:

C_1	2.514
C_2	0.8
C_3	0.55

S6. Chemistry set in the quasi-1D chemical kinetics model and 2D non-thermal plasma model

The full chemistry set used in the quasi-1D chemical kinetics model was recently developed and validated for a GA plasmatron by Vervloessem et al.[4] Table S3 lists all electron impact reactions. Most of these reactions are treated by energy-dependent cross sections. Table S4 lists the neutral-neutral reactions and the corresponding rate-coefficient expressions. For certain reactions, the rate coefficients of the vibrationally excited species are determined according to the Fridman-Macheret model in which the activation energy is lowered by αE_v, where α is the vibrational efficiency to lower the activation barrier and E_v is the vibrational energy. For those reactions, the α parameter is given in the last column of Table S4. Tables S5 to S6 list the electron-ion recombination, the ion-neutral and Table S.7 the ion-ion reactions and the corresponding rate coefficients, respectively. Table S8 displays the optical transitions. Reactions included in the reduced chemistry set of the 2D non-thermal plasma model are highlighted in blue bold face.

Table S3 Electron impact reactions implemented in the model for atomic and molecular nitrogen and oxygen species as well as NO_x species. The list includes vibrational excitation and de-excitation, electronic excitation and de-excitation, direct and dissociative ionization, dissociation, as well as direct and dissociative attachment reactions. These reactions are treated by energy-dependent cross sections when the rate coefficient is not specified in column 2. When indicated, rate coefficients are expressed in $cm^3\ s^{-1}$ or $cm^6\ s^{-1}$ for binary or ternary reactions, respectively.

Reaction	Rate Coefficient	Ref.	Note
$e^- + N_2 \leftrightarrow e^- + N_2(v)$		5	
$e^- + N_2(v) \leftrightarrow e^- + N_2(v')$		5	
$e^- + N_2(g,v) \rightarrow e^- + N_2(E_x)$		6	a, b, c
$e^- + N_2(E_x) \rightarrow e^- + N_2$		6	b
$e^- + N_2(g,v) \rightarrow 2e^- + N_2^+$		7	a
$e^- + N_2(E_x) \rightarrow 2e^- + N_2^+$		7	b
$e^- + N \rightarrow 2e^- + N^+$		8	
$e^- + N_2(g,v) \rightarrow 2e^- + N^+ + N$		9	a
$e^- + N_2(g,v) \rightarrow e^- + N + N$		6	a, c
$e^- + N_2(E_x) \rightarrow e^- + N + N$		6	b
$e^- + N \rightarrow e^- + N(E_x)$		6	d
$e^- + O_2 \leftrightarrow e^- + O_2(v)$		5	

$e^- + O_2(v) \leftrightarrow e^- + O_2(v')$		10	
$e^- + O_2(g,v) \rightarrow e^- + O_2(E_x)$		6	a, c, e
$e^- + O_2(E_x) \rightarrow e^- + O_2$		6	e
$e^- + O_2(g,v) \rightarrow 2e^- + O_2^+$		7	a, c
$e^- + O_2(E_x) \rightarrow 2e^- + O_2^+$		11	e
$e^- + O \rightarrow 2e^- + O^+$		6	
$e^- + O_2(g,v) \rightarrow 2e^- + O + O^+$		11	a, c
$e^- + O_2(E_x) \rightarrow 2e^- + O + O^+$		11	e
$e^- + O_3 \rightarrow 2e^- + O + O_2^+$		12	
$e^- + O_3 \rightarrow e^- + O^+ + O^- + O$		13	
$e^- + O_2(g,v) \rightarrow e^- + O + O$		6	a
$e^- + O_3 \rightarrow e^- + O_2 + O$		12	
$e^- + O_2(g,v) \rightarrow O + O^-$		6	a, c
$e^- + O_2(g,v) + M \rightarrow O_2^- + M$		14	a, c, f
$e^- + O_3 \rightarrow O^- + O_2$		7	
$e^- + O_3 \rightarrow O + O_2^-$		7	
$e^- + O_3 + M \rightarrow O_3^- + M$	5×10^{-31}	15	f
$e^- + O + M \rightarrow O^- + M$	1×10^{-31}	16	f
$e^- + NO \rightarrow 2e^- + NO^+$		17	
$e^- + NO_2 \rightarrow 2e^- + NO_2^+$		18	
$e^- + N_2O \rightarrow 2e^- + N_2O^+$		19	

$e^- + N_2O \rightarrow e^- + N_2 + O$		20	
$e^- + N_2O \rightarrow e^- + N_2 + O(1D)$		20	
$e^- + N_2O \rightarrow e^- + NO + N$		20	
$e^- + NO \rightarrow O^- + N$		17	
$e^- + N_2O \rightarrow N_2 + O^-$		19	
$e^- + NO_2 \rightarrow NO_2^-$	1×10^{-11}	21	
$e^- + NO_2 \rightarrow O^- + NO$	1×10^{-11}	22	
$e^- + NO + M \rightarrow NO^- + M$	8×10^{-31}	22	f
$e^- + N_2O + M \rightarrow N_2O^- + M$	6×10^{-33}	22	f

[a] For any species indicated with (g,v), g and v stand for its ground and vibrationally excited state, respectively.

[b] $N_2(E_x)$ represents the electronically excited states: $N_2(A^3\Sigma_u^+)$, $N_2(B^3\Pi_g)$, $N_2(C^3\Pi_u)$ and $N_2(a'^1\Sigma_u^-)$.

[c] The cross sections of the reactions involving excited species on the left hand side are shifted over the difference in the threshold energies.

[d] $N(E_x)$ represents the electronically excited states of atomic N: $N(2D)$ and $N(2P)$.

[e] $O_2(E_x)$ represents the electronically excited states: $O_2(a^1\Delta)$, $O_2(b^1\Sigma^+)$ and a combination of three states, i.e. $O_2(A^3\Sigma^+, C^3\Delta, c^1\Sigma^-)$ at a threshold energy of 4.5 eV.

[f] M represents any neutral species.

Table S4 Neutral-neutral reactions included in the model and the corresponding rate coefficient expressions. Tg is the gas temperature in K. The rate coefficients are expressed in $cm^3\ s^{-1}$ or $cm^6\ s^{-1}$ for binary or ternary reactions, respectively. For certain reactions, the rate coefficients of the vibrationally excited species are determined according to the Fridman-Macheret model in which the activation energy is lowered by αE_v, where α is the vibrational efficiency to lower the activation barrier and E_v is the vibrational energy. For those reactions, the α parameter is given in the last column.

Reaction	Rate coefficient	Ref.	Note
$N_2(g,v) + M \rightarrow N + N + M$	$8.37 \times 10^{-4} \times \left(\frac{T_g}{298}\right)^{-3.5} \times \exp$	23	a, b $\alpha = 1$
$N + N + M \rightarrow N_2 + M$	$1.38 \times 10^{-33} \times \exp\left(\frac{502.978}{T_g}\right)$	24	b
$N + N \rightarrow N_2^+ + e^-$	$2.7 \times 10^{-11} \times \exp\left(-\frac{6.74 \times 10^{}}{T_g}\right.$	22	
$N + N + N \rightarrow N_2\left(A^3\Sigma_u^+\right) + N$	1.0×10^{-32}	22	
$N + N + N \rightarrow N_2\left(B^3\Pi_g\right) + N$	1.4×10^{-32}	22	
$N + N + N_2 \rightarrow N_2\left(A^3\Sigma_u^+\right) + N_2$	1.7×10^{-33}	22	
$N + N + N_2 \rightarrow N_2\left(B^3\Pi_g\right) + N_2$	2.4×10^{-33}	22	
$N(2D) + M \rightarrow N + M$	2.4×10^{-14}	25	b
$N(2P) + N \rightarrow N(2D) + N$	1.8×10^{-12}	22	
$N(2P) + N_2 \rightarrow N + N_2$	2.0×10^{-18}	22	
$N_2\left(a'^1\Sigma_u^-\right) + N \rightarrow N_2 + N$	2.0×10^{-11}	25	
$N_2\left(a'^1\Sigma_u^-\right) + N_2 \rightarrow N_2 + N_2$	3.7×10^{-16}	25	
$N_2\left(a'^1\Sigma_u^-\right) + N_2 \rightarrow N_2\left(B^3\Pi_g\right) + N_2$	1.9×10^{-13}	22	
$N_2\left(a'^1\Sigma_u^-\right) + N_2\left(a'^1\Sigma_u^-\right) \rightarrow N_2^+ + N$	5.0×10^{-13}	25	
$N_2\left(a'^1\Sigma_u^-\right) + N_2\left(a'^1\Sigma_u^-\right) \rightarrow N_4^+ + e$	1.0×10^{-11}	22	

$N_2\left(a'^1\Sigma_u^-\right) + N_2\left(A^3\Sigma_u^+\right) \rightarrow N_4^+ + e$	4.0×10^{-12}	22	
$N_2\left(A^3\Sigma_u^+\right) + N \rightarrow N_2 + N(2P)$	$4.0 \times 10^{-11} \times \left(\frac{300}{T_g}\right)^{0.667}$	22	
$N_2\left(A^3\Sigma_u^+\right) + N \rightarrow N_2 + N$	2.0×10^{-12}	22	
$N_2\left(A^3\Sigma_u^+\right) + N_2 \rightarrow N_2 + N_2$	3.0×10^{-16}	22	
$N_2\left(A^3\Sigma_u^+\right) + N_2\left(a'^1\Sigma_u^-\right) \rightarrow N_2^+ + N_2$	1.0×10^{-12}	25	
$N_2\left(A^3\Sigma_u^+\right) + N_2\left(A^3\Sigma_u^+\right) \rightarrow N_2 + N_2($	2.0×10^{-12}	25	
$N_2\left(A^3\Sigma_u^+\right) + N_2\left(A^3\Sigma_u^+\right) \rightarrow N_2 + N_2($	3.0×10^{-10}	22	
$N_2\left(A^3\Sigma_u^+\right) + N_2\left(A^3\Sigma_u^+\right) \rightarrow N_2 + N_2($	1.5×10^{-10}	22	
$N_2\left(B^3\Pi_g\right) + N_2 \rightarrow N_2 + N_2$	2.0×10^{-12}	22	
$N_2\left(B^3\Pi_g\right) + N_2 \rightarrow N_2(A^3\Sigma_u^+) + N_2$	3×10^{-11}	22	
$N_2\left(C^3\Pi_u\right) + N_2 \rightarrow N_2 + \left(a'^1\Sigma_u^-\right)$	1.0×10^{-11}	22	
$O_2(g,v) + M \rightarrow O + O + M$	$\left(\frac{3.0 \times 10^{-6}}{T_g}\right) \times \exp\left(\frac{-59380}{T_g}\right)$		a $\alpha = 1$
$O + O + M \rightarrow O_2 + M$	$5.21 \times 10^{-35} \times \exp\left(\frac{900}{T_g}\right)$	26	b
$O + O_3 \rightarrow O_2 + O_2$	$8.0 \times 10^{-12} \times \exp\left(-\frac{2056}{T_g}\right)$	27	
$O + O_2(g,v) + M \rightarrow O_3 + M$	$1.34 \times 10^{-34} \times \left(\frac{T_g}{298}\right)^{-1.0}$	28	a, b

$O_3 + M \rightarrow O_2 + O + M$	$7.16 \times 10^{-10} \times \exp\left(-\frac{98120}{R_g T_g}\right)$	29	b, c
$O + O_2(E_x) + M \rightarrow O_3 + M$	$1.34 \times 10^{-34} \times \left(\frac{T_g}{298}\right)^{-1.0}$	28	b, d, e
$O + O_3 \rightarrow O_2 + O_2(a^1\Delta)$	$2.0 \times 10^{-11} \times \exp\left(-\frac{2280}{T_g}\right)$	22	
$O_2(a^1\Delta) + O \rightarrow O_2 + O$	7.0×10^{-16}	22	
$O_2(a^1\Delta) + O_2 \rightarrow O_2 + O_2$	$3.8 \times 10^{-18} \times \exp\left(-\frac{205}{T_g}\right)$	22	
$O_2(b^1\Sigma^+) + O \rightarrow O_2(a^1\Delta) + O$	8.1×10^{-14}	22	
$O_2(b^1\Sigma^+) + O \rightarrow O_2 + O(1D)$	$3.4 \times 10^{-11} \times \left(\frac{T_g}{300}\right)^{-0.1} \times \exp$	22	
$O_2(b^1\Sigma^+) + O_2 \rightarrow O_2 + O_2(a^1\Delta)$	$4.3 \times 10^{-22} \times (T_g)^{2.4} \times \exp\left(-$	22	
$O_2(b^1\Sigma^+) + O_3 \rightarrow O_2 + O_2 + O$	2.2×10^{-11}	22	
$O_2(a^1\Delta) + O_3 \rightarrow O_2 + O_2 + O(1D)$	$5.2 \times 10^{-11} \times \exp\left(-\frac{2840}{T_g}\right)$	22	
$O_2(a^1\Delta) + O_2(a^1\Delta) \rightarrow O_2 + O_2(b^1\Sigma^+$	$7.0 \times 10^{-28} \times (T_g)^{3.8} \times \exp\left(\frac{70}{T_g}\right.$	22	
$O(1D) + O \rightarrow O + O$	8.0×10^{-12}	22	
$O(1D) + O_2 \rightarrow O + O_2$	$6.4 \times 10^{-12} \times \exp\left(-\frac{67}{T_g}\right)$	22	
$O(1S) + O \rightarrow O(1D) + O(1D)$	$5.0 \times 10^{-11} \times \exp\left(-\frac{300}{T_g}\right)$	22	

$O(1S) + O_2 \rightarrow O + O_2$	$1.3 \times 10^{-12} \times \exp\left(-\frac{850}{T_g}\right)$	22	
$O(1S) + O_2 \rightarrow O + O + O$	3.0×10^{-12}	22	
$O(1S) + O_2(a^1\Delta) \rightarrow O + O + O$	3.2×10^{-11}	22	
$O(1S) + O_2(a^1\Delta) \rightarrow O(1D) + O_2(b^1\Sigma$	2.9×10^{-11}	22	
$O(1S) + O_2 \rightarrow O + O_2(A^3\Sigma^+, C^3\Delta, c^1\Sigma$	$3.0 \times 10^{-12} \times \exp\left(-\frac{850}{T_g}\right)$	22	f
$N + O_2(g,v) \rightarrow O + NO$	$2.36 \times 10^{-11} \times \exp\left(-\frac{44230}{R_g T_g}\right)$	30	a, c $\alpha = 0.$
$O + N_2(g,v) \rightarrow N + NO$	$3.01 \times 10^{-10} \times \exp\left(-\frac{318000}{R_g T_g}\right)$	31	a, c $\alpha = 1$
$O_3 + N \rightarrow NO + O_2$	$5.0 \times 10^{-12} \times \exp\left(-\frac{650}{T_g}\right)$	27	
$O_3 + NO \rightarrow O_2 + NO_2$	$2.5 \times 10^{-13} \times \exp\left(-\frac{765}{T_g}\right)$	22	
$O_3 + NO_2 \rightarrow O_2 + NO_3$	$1.2 \times 10^{-13} \times \exp\left(-\frac{2450}{T_g}\right)$	21	
$NO_3 + O_3 \rightarrow NO_2 + O_2 + O_2$	1.0×10^{-17}	32	
$N + NO \rightarrow O + N_2$	1.66×10^{-11}	33	
$N + NO_2 \rightarrow O + O + N_2$	9.1×10^{-13}	22	
$N + NO_2 \rightarrow O + N_2O$	3.0×10^{-12}	22	
$N + NO_2 \rightarrow N_2 + O_2$	7.0×10^{-13}	22	
$N + NO_2 \rightarrow NO + NO$	2.3×10^{-12}	22	
$O + NO \rightarrow N + O_2$	$7.5 \times 10^{-12} \times \left(\frac{T_g}{300}\right) \times \exp\left(-\frac{1}{}\right.$	22	

$O + NO_2 \rightarrow NO + O_2$	$9.05 \times 10^{-12} \times \left(\frac{T_g}{298}\right)^{-0.52}$	34	
$O + N_2O \rightarrow NO + NO$	$1.5 \times 10^{-10} \times \exp\left(-\frac{14090}{T_g}\right)$	22	
$O + N_2O \rightarrow N_2 + O_2$	$8.3 \times 10^{-12} \times \exp\left(-\frac{14000}{T_g}\right)$	22	
$O + NO_3 \rightarrow O_2 + N_2$	1.0×10^{-11}	22	
$NO + NO \rightarrow N + NO_2$	$3.3 \times 10^{-16} \times \left(\frac{300}{T_g}\right)^{0.5} \times \exp\left(-$	22	
$NO + NO \rightarrow O + N_2O$	$2.2 \times 10^{-12} \times \exp\left(-\frac{32100}{T_g}\right)$	22	
$NO + NO \rightarrow N_2 + O_2$	$5.1 \times 10^{-13} \times \exp\left(-\frac{33660}{T_g}\right)$	22	
$NO + N_2O \rightarrow N_2 + NO_2$	$4.6 \times 10^{-10} \times \exp\left(-\frac{25170}{T_g}\right)$	22	
$NO + NO_3 \rightarrow NO_2 + NO_2$	1.7×10^{-11}	22	
$NO_2 + NO_2 \rightarrow NO + NO_3$	$4.5 \times 10^{-10} \times \exp\left(-\frac{18500}{T_g}\right)$	22	
$NO_2 + NO_2 \rightarrow NO + NO + O_2$	$3.3 \times 10^{-12} \times \exp\left(-\frac{13500}{T_g}\right)$	22	
$NO_2 + NO_3 \rightarrow NO + NO_2 + O_2$	$2.3 \times 10^{-13} \times \exp\left(-\frac{1600}{T_g}\right)$	22	
$NO_3 + NO_3 \rightarrow O_2 + NO_2 + NO_2$	$4.3 \times 10^{-12} \times \exp\left(-\frac{3850}{T_g}\right)$	22	
$NO + O_2(g,v) \rightarrow O + NO_2$	$2.8 \times 10^{-12} \times \exp\left(-\frac{23400}{T_g}\right)$	22	a $\alpha = 1$

$NO + NO + O_2(g,v) \rightarrow NO_2 + NO_2$	$3.3 \times 10^{-39} \times \exp\left(-\frac{4410}{R_g T_g}\right)$	[35]	a, c $\alpha = 0.$
$NO_2 + O_2(g,v) \rightarrow NO + O_3$	$2.8 \times 10^{-12} \times \exp\left(-\frac{25400}{T_g}\right)$	[22]	a $\alpha = 0.$
$NO_3 + O_2(g,v) \rightarrow O_3 + NO_2$	$1.5 \times 10^{-12} \times \exp\left(-\frac{15020}{T_g}\right)$	[22]	a $\alpha = 0.$
$NO + O \rightarrow NO_2$	$3.01 \times 10^{-11} \times \left(\frac{T_g}{300}\right)^{-0.75}$	[36]	
$NO_2 + NO + M \rightarrow N_2O_3 + M$	$3.09 \times 10^{-34} \times \left(\frac{T_g}{300}\right)^{-7.70}$	[27]	b
$NO_2 + NO_2 + M \rightarrow N_2O_4 + M$	$1.4 \times 10^{-33} \times \left(\frac{T_g}{300}\right)^{-3.8}$	[27]	b
$NO_2 + NO_3 + M \rightarrow N_2O_5 + M$	$3.7 \times 10^{-30} \times \left(\frac{300}{T_g}\right)^{4.10}$	[35]	b
$N + O + M \rightarrow NO + M$	$1.0 \times 10^{-32} \times \left(\frac{300}{T_g}\right)^{0.5}$	[22]	b
$N_2(g,v) + O + M \rightarrow N_2O + M$	$3.9 \times 10^{-35} \times \exp\left(-\frac{10400}{T_g}\right)$	[22]	b
$N_2O + M \rightarrow N_2 + O + M$	$1.20 \times 10^{-9} \times \exp\left(-\frac{240000}{R_g T_g}\right)$	[22]	b, c
$NO_2 + M \rightarrow NO + O + M$	$9.4 \times 10^{-5} \times \left(\frac{T_g}{298}\right)^{-2.66} \times \exp($	[36]	b, c

$NO_3 + M \rightarrow NO + O_2 + M$	$2.51 \times 10^{-14} \times \exp\left(-\frac{10230}{R_g T_g}\right)$	37	b, c
$NO + M \rightarrow N + O + M$	$8.7 \times 10^{-9} \times \exp\left(-\frac{75994}{T_g}\right)$	22	b
$N_2O_3 + M \rightarrow NO + NO_2 + M$	$1.91 \times 10^{-7} \times \left(\frac{T_g}{298}\right)^{-8.7} \times \exp$	27	b, c
$N_2O_4 + M \rightarrow NO_2 + NO_3 + M$	$1.3 \times 10^{-5} \times \left(\frac{T_g}{298}\right)^{-3.8} \times \exp\left($	27	b, c
$N_2O_5 + M \rightarrow NO_2 + NO_3 + M$	$2.1 \times 10^{-11} \times \left(\frac{300}{T_g}\right)^{-3.5} \times \exp$	22	b, c
$NO + O_2(g,v) + M \rightarrow NO_3 + M$	$5.65 \times 10^{-41} \times \exp\left(-\frac{1750}{R_g T_g}\right)$	38	a, b, c
$NO + O_2(E_x) + M \rightarrow NO_3 + M$	$5.65 \times 10^{-41} \times \exp\left(-\frac{1750}{R_g T_g}\right)$	38	b, d
$N + N + NO \rightarrow N_2\left(A^3\Sigma^+_u\right) + NO$	1.7×10^{-33}	22	
$N + N + NO \rightarrow N_2\left(B^3\Pi_g\right) + NO$	2.4×10^{-33}	22	
$N + N + O \rightarrow N_2\left(A^3\Sigma^+_u\right) + O$	1.0×10^{-32}	22	
$N + N + O \rightarrow N_2\left(B^3\Pi_g\right) + O$	1.4×10^{-32}	22	
$N + N + O_2 \rightarrow N_2\left(A^3\Sigma^+_u\right) + O_2$	1.7×10^{-33}	22	
$N + N + O_2 \rightarrow N_2\left(B^3\Pi_g\right) + O_2$	2.4×10^{-33}	22	
$N(2D) + N_2O \rightarrow NO + N_2$	3.5×10^{-12}	22	
$N(2D) + NO \rightarrow N_2 + O$	1.8×10^{-10}	22	

$N(2D) + O \rightarrow N + O(1D)$	4.0×10^{-13}	22	
$N(2D) + O_2(g,v) \rightarrow NO + O$	5.2×10^{-12}	22	a
$N(2P) + NO \rightarrow N_2\left(A^3\Sigma_u^+\right) + O$	3.0×10^{-11}	22	
$N(2P) + O \rightarrow N + O$	1.0×10^{-12}	22	
$N(2P) + O_2(g,v) \rightarrow NO + O$	2.6×10^{-15}	22	a
$N_2\left(a'^1\Sigma_u^-\right) + NO \rightarrow N_2 + N + O$	3.6×10^{-10}	22	
$N_2\left(a'^1\Sigma_u^-\right) + O \rightarrow NO + N$	3.0×10^{-10}	31	
$N_2\left(a'^1\Sigma_u^-\right) + O_2(g,v) \rightarrow N_2 + O + O$	2.8×10^{-11}	22	a
$N_2\left(A^3\Sigma_u^+\right) + N_2O \rightarrow N_2 + N + NO$	1.0×10^{-11}	22	
$N_2\left(A^3\Sigma_u^+\right) + NO \rightarrow N_2 + NO$	6.9×10^{-11}	22	
$N_2\left(A^3\Sigma_u^+\right) + NO_2 \rightarrow N_2 + O + NO$	1.0×10^{-12}	22	
$N_2\left(A^3\Sigma_u^+\right) + O \rightarrow N_2 + O(1S)$	2.1×10^{-11}	22	
$N_2\left(A^3\Sigma_u^+\right) + O \rightarrow NO + N(2D)$	7.0×10^{-12}	22	
$N_2\left(A^3\Sigma_u^+\right) + O_2(g,v) \rightarrow N_2 + O + O$	$2.0 \times 10^{-12} \times \left(\frac{T_g}{300}\right)^{0.55}$	22	a
$N_2\left(A^3\Sigma_u^+\right) + O_2 \rightarrow N_2 + O_2(a^1\Delta)$	$2.0 \times 10^{-13} \times \left(\frac{T_g}{300}\right)^{0.55}$	22	
$N_2\left(A^3\Sigma_u^+\right) + O_2 \rightarrow N_2 + O_2$	2.54×10^{-12}	22	
$N_2\left(A^3\Sigma_u^+\right) + O_2(g,v) \rightarrow N_2O + O$	$2.0 \times 10^{-14} \times \left(\frac{T_g}{300}\right)^{0.55}$	22	a
$N_2\left(B^3\Pi_g\right) + N_2O \rightarrow N_2 + N + NO$	0.58×10^{-10}	39	
$N_2\left(B^3\Pi_g\right) + N_2O \rightarrow N_2 + N_2 + O$	0.58×10^{-10}	39	
$N_2\left(B^3\Pi_g\right) + O \rightarrow NO + N$	3.0×10^{-10}	31	

$N_2(C^3\Pi_u) + O \rightarrow NO + N$	3.0×10^{-10}	31	
$N_2(C^3\Pi_u) + O_2(g,v) \rightarrow N_2 + O + O$	3.0×10^{-10}	22	a
$NO + O_2(E_x) \rightarrow O + NO_2$	$2.8 \times 10^{-12} \times \exp\left(-\frac{23400}{T_g}\right)$	22	d, g
$NO_3 + O_2(E_x) \rightarrow O_3 + NO_2$	$1.5 \times 10^{-12} \times \exp\left(-\frac{15020}{T_g}\right)$	22	d, h
$O(1D) + N_2 \rightarrow N_2 + O$	2.3×10^{-11}	22	
$O(1S) + N \rightarrow O + N$	1.0×10^{-12}	22	
$O(1S) + N_2(g,v) \rightarrow O + N_2(g,v)$	1.0×10^{-17}	22	
$O_2(a^1\Delta) + N \rightarrow NO + O$	$2.0 \times 10^{-14} \times \exp\left(-\frac{600}{T_g}\right)$	22	
$O_2(a^1\Delta) + N_2(g,v) \rightarrow O_2 + N_2(g,v)$	3.0×10^{-21}	22	
$O_2(a^1\Delta) + NO \rightarrow O_2 + NO$	2.5×10^{-11}	22	
$O_2(b^1\Sigma^+) + N_2 \rightarrow O_2(a^1\Delta) + N_2$	$1.7 \times 10^{-15} \times \left(\frac{T_g}{300}\right)^{1.0}$	22	
$N_2(B^3\Pi_g) + NO \rightarrow N_2(A^3\Sigma^+_u) + NO$	2.4×10^{-10}	22	
$N_2(B^3\Pi_g) + O_2(g,v) \rightarrow N_2 + O + O$	3.0×10^{-10}	22	a

[a] For any species indicated with (g,v), g and v stand for its ground and vibrationally excited state, respectively.

[b] M represents any neutral species.

[c] $R_g = 8.3144598\, J.K^{-1}.mol^{-1}$ is the universal gas constant.

[d] $O_2(E_x)$ represents the two electronically excited states: $O_2(a^1\Delta)$ and $O_2(b^1\Sigma^+)$.

[e] The rate coefficient is assumed to be equal to the rate of $O + O_2 + M \rightarrow O_3 + M$.

[f] $O_2(A^3\Sigma^+, C^3\Delta, c^1\Sigma^-)$ is a combination of three electronic excited states at a threshold energy of 4.5 eV.

[g] The rate coefficient is assumed to be equal to the rate of $NO + O_2 \rightarrow O + NO_2$.

[h] The rate coefficient is assumed to be equal to the rate of $NO_3 + O_2 \rightarrow O_3 + NO_2$.

Table S5 Electron-ion recombination reactions included in the model and the corresponding rate coefficient expressions. Te is to the electron temperature in K and Tg is the gas temperature in K. The rate coefficients are expressed in $cm^3\ s^{-1}$ or $cm^6\ s^{-1}$ for binary or ternary reactions, respectively.

Reaction	Rate coefficient	Ref.	Note
$e^- + N_2^+ \rightarrow N + N_{(g,\ E_x)}$	$R \times 1.8 \times 10^{-7} \times \left(\frac{300}{T_e}\right)^{0.39}$	22	a
$e^- + N_3^+ \rightarrow N_2 + N$	$2 \times 10^{-7} \times \left(\frac{300}{T_e}\right)^{0.5}$	40	
$e^- + N_3^+ \rightarrow N_2(E_x) + \mathrm{N}$	$6.91 \times 10^{-8} \times \left(\frac{T_e}{11604.5}\right)^{-0.5}$	40	c
$e^- + N_4^+ \rightarrow N_2 + N_2$	$2.3 \times 10^{-6} \times \left(\frac{300}{T_e}\right)^{0.53}$	22	
$e^- + N_4^+ \rightarrow N_2 + N + N$	$3.13 \times 10^{-7} \times \left(\frac{T_e}{11604.5}\right)^{-0.41}$	40	
$e^- + N^+ + e^- \rightarrow e^- + N$	$7 \times 10^{-20} \times \left(\frac{300}{T_e}\right)^{4.5}$	40	
$e^- + N^+ + M \rightarrow N + M$	$6 \times 10^{-27} \times \left(\frac{300}{T_e}\right)^{1.5}$	41	b
$e^- + N_2^+ + e^- \rightarrow e^- + N_2$	$1 \times 10^{-19} \times \left(\frac{T_e}{300}\right)^{-4.5}$	40	
$e^- + N_2^+ + M \rightarrow N_2 + M$	$2.49 \times 10^{-29} \times \left(\frac{T_e}{11604.5}\right)^{-1.5}$	40	b
$e^- + O^+ + O_2 \rightarrow O + O_2$	$6 \times 10^{-27} \times \left(\frac{300}{T_e}\right)^{1.5}$	41	
$e^- + O^+ + e^- \rightarrow e^- + O$	$7 \cdot 10^{-20} \cdot \left(\frac{300}{T_e}\right)^{4.5}$	22	
$e^- + O_2^+ + M \rightarrow O_2 + M$	1×10^{-26}	16	b
$e^- + O_2^+ + e^- \rightarrow e^- + O_2$	$1 \times 10^{-19} \times \left(\frac{T_e}{300}\right)^{-4.5}$	41	

$e^- + O_2^+ \rightarrow O + O$	$6.46 \times 10^{-5} \times T_e^{-0.5} \times T_g^{-0.5}$	42	
$e^- + O_2^+ \rightarrow O + O(1D)$	$1.08 \times 10^{-7} \left(\frac{T_e}{300}\right)^{-0.7}$	22	
$e^- + O_2^+ \rightarrow O + O(1S)$	$0.14 \times 10^{-7} \left(\frac{T_e}{300}\right)^{-0.7}$	22	
$e^- + O_4^+ \rightarrow O_2 + O_2$	$1.4 \times 10^{-6} \times \left(\frac{300}{T_e}\right)^{0.5}$	22	
$e^- + NO^+ + e^- \rightarrow e^- + NO$	$1.0 \times 10^{-19} \left(\frac{T_e}{300}\right)^{-4.5}$	41	
$e^- + NO^+ + M \rightarrow NO + M$	$2.49 \times 10^{-29} \times \left(\frac{T_e}{11604.5}\right)^{-1.5}$	40	b
$e^- + NO^+ \rightarrow O + N(g,E_x)$	$R \times 4.2 \times 10^{-7} \times \left(\frac{300}{T_e}\right)^{0.85}$	22	d
$e^- + N_2O^+ \rightarrow N_2 + O$	$2.0 \times 10^{-7} \times \left(\frac{300}{T_e}\right)^{0.5}$	22	
$e^- + NO_2^+ \rightarrow NO + O$	$2.0 \times 10^{-7} \times \left(\frac{300}{T_e}\right)^{0.5}$	22	
$e^- + O_2^+ N_2 \rightarrow O_2 + N_2$	$1.3 \times 10^{-6} \times \left(\frac{300}{T_e}\right)^{0.5}$	22	

[a] In N(g, E_x), g stands for the ground state of atomic N and E_x represents two of its electronically excited states: $N(2D)$ and $N(2P)$; R is equal to 0.5, 0.45 and 0.05 for N, $N(2D)$ and $N(2P)$, respectively.

[b] M represents any neutral species.

[c] $N_2(E_x)$ represents $N_2(A^3\Sigma_u^+)$ and $N_2(B^3\Pi_g)$.

[d] In $N(g,E_x)$, g stands for the ground state of atomic N and E_x represents the electronic excited state $N(2D)$; R is equal to 0.2 and 0.8 for N and $N(2D)$, respectively.

Table S6 Ion-neutral reactions included in the model and the corresponding rate coefficient expressions. T_g is the gas temperature in K. For certain reactions, T_{ion} is the effective temperature of the reacting ion in K [26]. The rate coefficients are expressed in $cm^3\ s^{-1}$ or $cm^6\ s^{-1}$ for binary or ternary reactions, respectively.

Reaction	Rate coefficient	Ref.	Note
$N_2^+ + N \rightarrow N^+ + N_2$	$7.2 \times 10^{-13} \times \left(\frac{T_{ion}}{300}\right)$	22	
$N_2^+ + N + N_2 \rightarrow N_3^+ + N_2$	$9.0 \times 10^{-30} \times \left(\frac{400}{T_{ion}}\right)$	22	
$N_4^+ + N_2 \rightarrow N_2^+ + N_2 + N_2$	$2.1 \times 10^{-16} \times \left(\frac{Tion}{121}\right)$	22	
$N^+ + N_2 + N_2 \rightarrow N_3^+ + N_2$	$1.7 \times 10^{-29} \times \left(\frac{300}{Tion}\right)^{2.1}$	22	
$N_2^+ + N_2 + N_2 \rightarrow N_4^+ + N_2$	$5.2 \times 10^{-29} \times \left(\frac{300}{T_{ion}}\right)^{2.2}$	22	
$N^+ + N + N_2 \rightarrow N_2^+ + N_2$	1.0×10^{-29}	22	
$N^+ + N \rightarrow N_2^+$	1.0×10^{-29}	43	
$N_3^+ + N \rightarrow N_2^+ + N_2$	6.6×10^{-11}	22	
$N_4^+ + N \rightarrow N^+ + N_2 + N_2$	1.0×10^{-11}	22	
$N_2^+ + N_2\left(A^3\Sigma_u^+\right) \rightarrow N_3^+ + N$	3.0×10^{-10}	21	
$O^- + M \rightarrow O + M + e^-$	4.0×10^{-12}	21	a
$O^- + O \rightarrow O_2 + e^-$	2.3×10^{-10}	44	
$O^- + O_2(g,v) + M \rightarrow O_3^- + M$	$1.1 \times 10^{-30} \times \exp\left(\frac{300}{T_g}\right)$	44	a, b
$O^- + O_2(g,v) \rightarrow O_3 + e^-$	5.0×10^{-15}	22	b
$O^- + O_3 \rightarrow O_2 + O_2 + e^-$	3.0×10^{-10}	45	
$O^- + O_3 \rightarrow O_3^- + O$	5.3×10^{-10}	46	

$O^+ + O + M \rightarrow O_2^+ + M$	1.0×10^{-29}	[41]	a
$O^+ + O_2(g,v) \rightarrow O + O_2^+$	$1.9 \times 10^{-11} \times \left(\frac{T_g}{300}\right)^{-0.5}$	[47]	b
$O^+ + O_3 \rightarrow O_2^+ + O_2$	1.0×10^{-10}	[41]	
$O_2^- + M \rightarrow O_2 + M + e^-$	$2.7 \times 10^{-10} \times \left(\frac{T_g}{300}\right)^{0.5} \times \exp($	[47]	a
$O_2^- + O \rightarrow O_2 + O^-$	3.31×10^{-10}	[44]	
$O_2^- + O_2(g,v) + M \rightarrow O_4^- + M$	$3.5 \times 10^{-31} \times \left(\frac{T_g}{300}\right)^{-1.0}$	[41,44,46]	a, b
$O_2^- + O_2 \rightarrow O_2 + O_2 + e^-$	2.18×10^{-18}	[48]	
$O_2^- + O_3 \rightarrow O_3^- + O_2$	4.0×10^{-10}	[44]	
$O_2^+ + O_2(g,v) + M \rightarrow O_4^+ + M$	$2.4 \times 10^{-30} \times \left(\frac{T_g}{300}\right)^{-3.2}$	[41]	a, b
$O_3^- + M \rightarrow O_3 + M + e^-$	2.3×10^{-11}	[47]	a
$O_3^- + O \rightarrow O_2 + O_2 + e^-$	1.0×10^{-13}	[46]	
$O_3^- + O \rightarrow O_2^- + O_2$	2.5×10^{-10}	[15]	
$O_3^- + O \rightarrow O_3 + O^-$	1.0×10^{-13}	[44]	
$O_3^- + O_3 \rightarrow O_2 + O_2 + O_2 + e^-$	3.0×10^{-10}	[46]	
$O_4^- + O \rightarrow O^- + O_2 + O_2$	3.0×10^{-10}	[41]	
$O_4^- + O \rightarrow O_3^- + O_2$	4.0×10^{-10}	[41]	
$O_4^- + O_2 \rightarrow O_2^- + O_2 + O_2$	$1.0 \times 10^{-10} \times \exp\left(-\frac{1044}{T_g}\right)$	[22]	
$O_4^+ + O \rightarrow O_2^+ + O_3$	3.0×10^{-10}	[41]	

$O_4^+ + O_2 \rightarrow O_2^+ + O_2 + O_2$	$3.3 \times 10^{-6} \times \left(\frac{300}{T_g}\right)^{4.0} \times \exp\left($	[41]	
$O^- + O_2(a^1\Delta) \rightarrow O_3 + e^-$	3.0×10^{-10}	[22]	
$O_2^- + O_2(a^1\Delta) \rightarrow O_2 + O_2 + e^-$	2.0×10^{-10}	[22]	
$O_2^- + O_2(b^1\Sigma^+) \rightarrow O_2 + O_2 + e^-$	3.6×10^{-10}	[22]	
$O_2^+ + O_2(E_x) + M \rightarrow O_4^+ + M$	$2.4 \times 10^{-30} \times \left(\frac{T_g}{300}\right)^{-3.2}$	[22]	a, c, d
$O_4^+ + O_2(a^1\Delta) \rightarrow O_2^+ + O_2 + O_2$	1.0×10^{-10}	[22]	
$O_4^- + O_2(E_x) \rightarrow O_2^- + O_2 + O_2$	1.0×10^{-10}	[22]	c
$O^- + O_2(a^1\Delta) \rightarrow O_2^- + O$	1.0×10^{-10}	[22]	
$O^- + O_2(E_x) + M \rightarrow O_3^- + M$	$1.1 \times 10^{-30} \times \exp\left(\frac{300}{T_g}\right)$	[22]	a, c, e
$O_2^- + O_2(E_x) + M \rightarrow O_4^- + M$	$3.5 \times 10^{-31} \times \exp\left(\frac{T_g}{300}\right)^{-1.0}$	[41]	a, c, f
$N^+ + N + O_2 \rightarrow N_2^+ + O_2$	1.0×10^{-29}	[22]	
$N^+ + N_2O \rightarrow NO^+ + N_2$	5.5×10^{-10}	[22]	
$N^+ + NO \rightarrow N_2^+ + O$	3.0×10^{-12}	[22]	
$N^+ + NO \rightarrow NO^+ + N$	8.0×10^{-10}	[22]	
$N^+ + NO \rightarrow O^+ + N_2$	1.0×10^{-12}	[22]	
$N^+ + O + M \rightarrow NO^+ + M$	1.0×10^{-29}	[22]	a
$N^+ + O \rightarrow N + O^+$	1.0×10^{-12}	[22]	
$N^+ + O_2 \rightarrow NO^+ + O$	2.5×10^{-10}	[22]	
$N^+ + O_2 \rightarrow O^+ + NO$	2.8×10^{-11}	[22]	

$N^+ + O_2 \rightarrow O_2^+ + N$	2.8×10^{-10}	22	
$N^+ + O_3 \rightarrow NO^+ + O_2$	5.0×10^{-10}	22	
$N_2^+ + N_2O \rightarrow N_2O^+ + N_2$	5.0×10^{-10}	22	
$N_2^+ + N_2O \rightarrow NO^+ + N + N_2$	4.0×10^{-10}	22	
$N_2^+ + NO \rightarrow NO^+ + N_2$	3.3×10^{-10}	22	
$N_2^+ + O \rightarrow NO^+ + N$	$1.3 \times 10^{-10} \times \left(\frac{300}{T_{ion}}\right)^{0.5}$	22	
$N_2^+ + O_2 \rightarrow O_2^+ + N_2$	$6.0 \times 10^{-11} \times \left(\frac{300}{T_{ion}}\right)^{0.5}$	22	
$N_2^+ + O_3 \rightarrow O_2^+ + O + N_2$	1.0×10^{-10}	22	
$N_2O^- + N \rightarrow NO + N_2 + e^-$	5.0×10^{-10}	21	
$N_2O^- + O \rightarrow NO + NO + e^-$	1.5×10^{-10}	21	
$N_2O^+ + NO \rightarrow NO^+ + N_2O$	2.9×10^{-10}	22	
$N_3^+ + NO \rightarrow N_2O^+ + N_2$	7.0×10^{-11}	22	
$N_3^+ + NO \rightarrow NO^+ + N + N_2$	7.0×10^{-11}	22	
$N_3^+ + O_2 \rightarrow NO_2^+ + N_2$	4.4×10^{-11}	22	
$N_3^+ + O_2 \rightarrow O_2^+ + N + N_2$	2.3×10^{-11}	22	
$N_4^+ + NO \rightarrow NO^+ + N_2 + N_2$	4.0×10^{-10}	22	
$N_4^+ + O \rightarrow O^+ + N_2 + N_2$	2.5×10^{-10}	22	
$N_4^+ + O_2 \rightarrow O_2^+ + N_2 + N_2$	2.5×10^{-10}	22	
$NO^- + N_2O \rightarrow NO + N_2O + e^-$	$4.26 \times 10^{-10} \times \exp\left(-\frac{107.2}{T_g}\right)$	49	

$NO^- + NO \rightarrow NO + NO + e^-$	$3.28 \times 10^{-10} \times \exp\left(-\frac{105.1}{T_g}\right)$	[49]	
$NO^- + N \rightarrow N_2O + e^-$	5.0×10^{-10}	[22]	
$NO^- + N_2O \rightarrow NO_2^- + N_2$	2.8×10^{-14}	[22]	
$NO^- + NO_2 \rightarrow NO_2^- + NO$	7.4×10^{-10}	[22]	
$NO^- + O \rightarrow NO_2 + e^-$	1.5×10^{-10}	[21]	
$NO^- + O_2 \rightarrow O_2^- + NO$	5.0×10^{-10}	[22]	
$NO_2^- + N \rightarrow NO + NO + e^-$	5.0×10^{-10}	[21]	
$NO_2^- + N_2O_5 \rightarrow NO_3^- + NO_2 + NO_2$	7.0×10^{-10}	[22]	
$NO_2^- + NO_2 \rightarrow NO_3^- + NO$	4.0×10^{-12}	[22]	
$NO_2^- + NO_3 \rightarrow NO_3^- + NO_2$	5.0×10^{-10}	[22]	
$NO_2^- + O_3 \rightarrow NO_3^- + O_2$	1.8×10^{-11}	[22]	
$NO_2^+ + NO \rightarrow NO^+ + NO_2$	2.9×10^{-10}	[22]	
$NO_3^- + N \rightarrow NO + NO_2 + e^-$	5.0×10^{-10}	[21]	
$NO_3^- + NO \rightarrow NO_2^- + NO_2$	3.0×10^{-15}	[22]	
$NO_3^- + O \rightarrow NO + O_3 + e^-$	1.5×10^{-10}	[21]	
$O^- + N \rightarrow NO + e^-$	2.6×10^{-10}	[22]	
$O^- + N_2(g,v) \rightarrow N_2O + e^-$	0.5×10^{-13}	[22]	b
$O^- + N_2\left(A^3\Sigma_u^+\right) \rightarrow O + N_2 + e^-$	2.2×10^{-9}	[22]	
$O^- + N_2\left(B^3\Pi_g\right) \rightarrow O + N_2 + e^-$	1.9×10^{-9}	[22]	
$O^- + N_2O \rightarrow N_2O^- + O$	2.0×10^{-12}	[22]	

$O^- + N_2O \rightarrow NO^- + NO$	2.0×10^{-10}	[22]	
$O^- + NO + M \rightarrow NO_2^- + M$	1.0×10^{-29}	[22]	a
$O^- + NO \rightarrow NO_2 + e^-$	2.6×10^{-10}	[22]	
$O^- + NO_2 \rightarrow NO_2^- + O$	1.2×10^{-9}	[22]	
$O^+ + N + M \rightarrow NO^+ + M$	1.0×10^{-29}	[22]	a
$O^+ + N \rightarrow N^+ + O$	1.3×10^{-10}	[22]	
$O^+ + N_2(g,v) + M \rightarrow NO^+ + N + M$	$6.0 \times 10^{-29} \times \left(\frac{300}{T_{ion}}\right)^2$	[22]	a, b
$O^+ + N_2(g,v) \rightarrow NO^+ + N$	$\left(1.5 - 2.0 \times 10^{-3} \times T_{ion} + 9.6\right.$	[22]	b
$O^+ + N_2O \rightarrow N_2O^+ + O$	2.2×10^{-10}	[22]	
$O^+ + N_2O \rightarrow NO^+ + NO$	2.3×10^{-10}	[22]	
$O^+ + N_2O \rightarrow O_2^+ + N_2$	2.0×10^{-11}	[22]	
$O^+ + NO \rightarrow NO^+ + O$	2.4×10^{-11}	[22]	
$O^+ + NO \rightarrow O_2^+ + N$	3.0×10^{-12}	[22]	
$O^+ + NO_2 \rightarrow NO_2^+ + O$	1.6×10^{-9}	[22]	
$O_2^- + N \rightarrow NO_2 + e^-$	5.0×10^{-10}	[22]	
$O_2^- + N_2\left(B^3\Pi_g\right) \rightarrow O_2 + N_2 + e^-$	2.5×10^{-9}	[22]	
$O_2^- + N_2\left(A^3\Sigma_u^+\right) \rightarrow O_2 + N_2 + e^-$	2.1×10^{-9}	[22]	
$O_3^- + N_2\left(B^3\Pi_g\right) \rightarrow O_3 + N_2 + e^-$	2.5×10^{-9}	[21]	
$O_3^- + N_2\left(A^3\Sigma_u^+\right) \rightarrow O_3 + N_2 + e^-$	2.1×10^{-9}	[21]	
$NO^- + N_2\left(B^3\Pi_g\right) \rightarrow NO + N_2 + e^-$	2.5×10^{-9}	[21]	

$NO^- + N_2(A^3\Sigma_u^+) \rightarrow NO + N_2 + e^-$	2.1×10^{-9}	21	
$N_2O^- + N_2(B^3\Pi_g) \rightarrow N_2O + N_2 + e$	2.5×10^{-9}	21	
$N_2O^- + N_2(A^3\Sigma_u^+) \rightarrow N_2O + N_2 +$	2.1×10^{-9}	21	
$NO_2^- + N_2(B^3\Pi_g) \rightarrow NO_2 + N_2 + e^-$	2.5×10^{-9}	21	
$NO_2^- + N_2(A^3\Sigma_u^+) \rightarrow NO_2 + N_2 + e$	2.1×10^{-9}	21	
$NO_3^- + N_2(B^3\Pi_g) \rightarrow NO_3 + N_2 + e^-$	2.5×10^{-9}	21	
$NO_3^- + N_2(A^3\Sigma_u^+) \rightarrow NO_3 + N_2 + e$	2.1×10^{-9}	21	
$O_2^- + NO_2 \rightarrow NO_2^- + O_2$	7.0×10^{-10}	22	
$O_2^- + NO_3 \rightarrow NO_3^- + O_2$	5.0×10^{-10}	22	
$O_2^+ + N \rightarrow NO^+ + O$	1.2×10^{-10}	22	
$O_2^+ + N_2(g,v) + N_2 \rightarrow O_2^+N_2 + N_2$	$9.0 \times 10^{-31} \times \left(\frac{300}{T_{ion}}\right)^2$	22	b
$O_2^+ + N_2(g,v) \rightarrow NO^+ + NO$	1.0×10^{-17}	22	b
$O_2^+ + NO \rightarrow NO^+ + O_2$	6.3×10^{-10}	22	
$O_2^+ + NO_2 \rightarrow NO^+ + O_3$	1.0×10^{-11}	22	
$O_2^+ + NO_2 \rightarrow NO_2^+ + O_2$	6.6×10^{-10}	22	
$O_2^+N_2 + N_2 \rightarrow O_2^+ + N_2 + N_2$	$1.1 \times 10^{-6} \times \left(\frac{300}{T_{ion}}\right)^{5.3} \times \exp($	22	
$O_2^+N_2 + O_2 \rightarrow O_4^+ + N_2$	1.0×10^{-9}	22	
$O_3^- + N \rightarrow NO + O_2 + e^-$	5.0×10^{-10}	21	
$O_3^- + NO \rightarrow NO_2^- + O_2$	2.6×10^{-12}	22	
$O_3^- + NO \rightarrow NO_3^- + O$	1.0×10^{-11}	22	

$O_3^- + NO_2 \rightarrow NO_2^- + O_3$	7.0×10^{-11}	[22]	
$O_3^- + NO_2 \rightarrow NO_3^- + O_2$	2.0×10^{-11}	[22]	
$O_3^- + NO_3 \rightarrow NO_3^- + O_3$	5.0×10^{-10}	[22]	
$O_4^- + N_2 \rightarrow O_2^- + O_2 + N_2$	$1 \times 10^{-10} \times \exp\left(-\frac{1044}{T_g}\right)$	[22]	
$O_4^- + NO \rightarrow NO_3^- + O_2$	2.5×10^{-10}	[22]	
$O_4^+ + N_2(g,v) \rightarrow O_2^+ N_2 + O_2$	$4.6 \times 10^{-12} \times \left(\frac{T_{ion}}{300}\right)^{2.5} \times \exp($	[22]	b
$O_4^+ + NO \rightarrow NO^+ + O_2 + O_2$	1.0×10^{-10}	[22]	

[a] M represents any neutral species.

[b] For any species indicated with (g,v), g and v stand for its ground and vibrationally excited state, respectively.

[c] $O_2(E_x)$ represents the electronically excited states: $O_2(a^1\Delta)$ and $O_2(b^1\Sigma^+)$.

[d] The rate coefficient is assumed to be equal to the rate of $O_2^+ + O_2 + M \rightarrow O_4^+ + M$.

[e] The rate coefficient is assumed to be equal to the rate of $O^- + O_2 + M \rightarrow O_3^- + M$.

[f] The rate coefficient is assumed to be equal to the rate of $O_2^- + O_2 + M \rightarrow O_4^- + M$.

Table S7 Ion-ion reactions included in the model, the corresponding rate coefficient expressions and the references. T_g is the gas temperature in K. The rate coefficients are expressed in $cm^3\ s^{-1} or\ cm^6\ s^{-1}$ for binary or ternary reactions, respectively.

Reaction	Rate coefficient	Ref.	Note
$O^- + O^+ + M \rightarrow O_2 + M$	$1.0 \times 10^{-25} \times \left(\frac{300}{T_g}\right)^{2.5}$	47	a
$O^- + O_2^+ + M \rightarrow O_3 + M$	$1.0 \times 10^{-25} \times \left(\frac{300}{T_g}\right)^{2.5}$	47	a
$O_2^- + O^+ + M \rightarrow O_3 + M$	$1.0 \times 10^{-25} \times \left(\frac{300}{T_g}\right)^{2.5}$	47	a
$O_2^- + O_2^+ + M \rightarrow O_2 + O_2 + M$	$1.0 \times 10^{-25} \times \left(\frac{300}{T_g}\right)^{2.5}$	47	a
$O_3^- + O^+ + M \rightarrow O_3 + O + M$	$2.0 \times 10^{-25} \times \left(\frac{300}{T_g}\right)^{2.5}$	21	a
$O_3^- + O_2^+ + M \rightarrow O_3 + O_2 + M$	$2.0 \times 10^{-25} \times \left(\frac{300}{T_g}\right)^{2.5}$	21	a
$O^- + O_2^+ \rightarrow O + O + O$	$2.60 \times 10^{-8} \times \left(\frac{300}{T_g}\right)^{0.44}$	44	a
$O_3^- + O_2^+ \rightarrow O + O + O_3$	$1.0 \times 10^{-7} \times \left(\frac{300}{T_g}\right)^{0.5}$	44	a
$O^- + O^+ \rightarrow O + O$	$4.0 \times 10^{-8} \times \left(\frac{300}{T_g}\right)^{0.43}$	44	
$O^- + O_2^+ \rightarrow O_2 + O$	$2.6 \times 10^{-8} \times \left(\frac{300}{T_g}\right)^{0.44}$	44	
$O_2^- + O^+ \rightarrow O + O_2$	$2.7 \times 10^{-7} \times \left(\frac{300}{T_g}\right)^{0.5}$	44	
$O_2^- + O_2^+ \rightarrow O_2 + O_2$	$2.01 \times 10^{-7} \times \left(\frac{300}{T_g}\right)^{0.5}$	44	

$O_2^- + O_2^+ \rightarrow O_2 + O + O$	$1.01 \times 10^{-13} \times \left(\frac{300}{T_g}\right)^{0.5}$	44	
$O_3^- + O^+ \rightarrow O_3 + O$	$1.0 \times 10^{-7} \times \left(\frac{300}{T_g}\right)^{0.5}$	48	
$O_3^- + O_2^+ \rightarrow O_2 + O_3$	$2.0 \times 10^{-7} \times \left(\frac{300}{T_g}\right)^{0.5}$	44	
$NO^- + A^+ + M \rightarrow NO + A + M$	$2.0 \times 10^{-25} \times \left(\frac{300}{T_g}\right)^{2.5}$	21	a, b
$NO_2^- + A^+ + M \rightarrow NO_2 + A + M$	$2.0 \times 10^{-25} \times \left(\frac{300}{T_g}\right)^{2.5}$	21	a, b
$N_2O^- + A^+ + M \rightarrow N_2O + A + M$	$2.0 \times 10^{-25} \times \left(\frac{300}{T_g}\right)^{2.5}$	21	a, b
$NO_3^- + A^+ + M \rightarrow NO_3 + A + M$	$2.0 \times 10^{-25} \times \left(\frac{300}{T_g}\right)^{2.5}$	21	a, b
$O_3^- + B^+ + M \rightarrow O_3 + B + M$	$2.0 \times 10^{-25} \times \left(\frac{300}{T_g}\right)^{2.5}$	21	a, c

[a] M represents any neutral species.

[b] A represents N, O, N_2, O_2, NO, NO_2 and N_2O species.

[c] B represents N, N_2, NO, NO_2 and N_2O species.

Table S8 Optical transitions of N_2 and O_2 species. The rate coefficients are expressed in s^{-1}.

Reaction	Rate coefficient	Ref.	Note
$N_2(A^3\Sigma_u^+) \rightarrow N_2$	0.5	22	
$N_2(B^3\Pi_g) \rightarrow N_2(A^3\Sigma_u^+)$	1.35×10^5	22	
$N_2(a'^1\Sigma_u^-) \rightarrow N_2$	1.0×10^2	22	
$N_2(C^3\Pi_u) \rightarrow N_2(B^3\Pi_g)$	2.45×10^7	22	
$O_2(a^1\Delta) \rightarrow O_2$	2.6×10^{-4}	22	
$O_2(b^1\Sigma^+) \rightarrow O_2$	8.5×10^{-2}	22	
$O_2(b^1\Sigma^+) \rightarrow O_2(a^1\Delta)$	1.5×10^{-3}	22	
$O_2(A^3\Sigma^+, C^3\Delta, c^1\Sigma^-) \rightarrow O_2$	11	22	a

[a] $O_2(A^3\Sigma^+, C^3\Delta, c^1\Sigma^-)$ is a combination of three electronic excited states at a threshold energy of 4.5 eV.

The reaction rate coefficient expressions of the VT relaxations and VV exchanges between N_2 - N_2, N_2 - O_2 and O_2 - O_2 are calculated using the Forced Harmonic Oscillator (FHO) model proposed by Adamovich et al.[50] This method offers a semi-classical non-perturbative analytical solution for VT and VV transitions of diatomic molecules by averaging the VT and VV probabilities (P_{VT} and P_{VV}) over the one-dimensional Boltzmann distribution.

$$P_{VT}(i \rightarrow f) = \frac{(n_s)^s}{(s!)^2} \cdot \varepsilon^s \cdot exp\left(-\frac{2n_s}{s+1}\varepsilon\right) \quad (18)$$

$$P_{VV}(i_1, i_2 \rightarrow f_1, f_2) \tilde{=} \frac{\left[n_s^{(1)} n_s^{(2)}\right]^s}{(s!)^2} \cdot \left(\frac{\rho_\varepsilon^2}{4}\right)^s \cdot exp\left[-\frac{2n_s^{(1)} n_s^{(2)} \rho_\varepsilon^2}{s+1 \quad 4}\right] \quad (19)$$

with $s = |i - f|$, $n_s = \left[\frac{\max(i,f)!}{\min(i,f)!}\right]^{1/s}$. ρ_ε and ε are collision and potential specific parameters.

Table S. 9 Vibrational –vibrational exchanges and vibrational-translational relaxations for N_2 (as an example) and the rate coefficient expression.

Reaction	Rate coefficient
$N_2(v_i) + M \rightarrow N_2(v_i - 1) + M$	$Z \cdot \left(\frac{m}{kT}\right) \int_0^\infty P_{VT}(\bar{v}) \cdot exp\left(\frac{-mv^2}{2kT}\right) vdv$
$N_2(v_i) + N_2(v_j) \rightarrow N_2(v_i - 1) + N_2(v_j + 1)$	$Z \cdot \left(\frac{m}{kT}\right) \int_0^\infty P_{VV}(\bar{v}) \cdot exp\left(\frac{-mv^2}{2kT}\right) vdv$

M represents any neutral particle in the plasma.
v_i and v_j are the vibrational levels of N_2 (0-24).
Z is the collision frequency and v is the particle velocity.

The reaction rate coefficients of the VT relaxations between N_2 – N are based on quasi-classical calculations that have been reproduced through a fit as proposed by Esposito et al.[51], for the following general reaction:

$N_2(v) + N \rightarrow N_2(w) + N$, with $v > w$

All the relevant trends in the rate coefficients were taken into consideration by using an additive model into the exponential argument of the reaction rate coefficient, as shown in the following expression (valid for $v = 1 - 66$ and $\Delta v = 1 - 30$):

$$K(v,T,\Delta v) = \exp\left(a_1(v,\Delta v) + \frac{a_2(v,\Delta v)}{T} + \frac{a_3(v,\Delta v)}{T^2} + \frac{a_4(v,\Delta v)}{T^3} + a_5(v,\Delta v) \cdot \ln(T)\right) \quad (20)$$

where

$$a_i(v,\Delta v) = z_{i0}(\Delta v) + z_{i1}(\Delta v)v + z_{i2}(\Delta v)v^2 + z_{i3}(\Delta v)v^3 + z_{i4}(\Delta v)v^4 \quad (21)$$

$$z_{ij}(\Delta v) = b_{ij} + c_{ij}\Delta v \quad (22)$$

For which the parameters are reported in [51].

Similarly, the reaction rate coefficients of the VT relaxations between O_2 – O are based on quasi-classical calculations that have been reproduced through a fit as proposed by Esposito et al.[52], for the following general reaction:

$O_2(v) + O \rightarrow O_2(w) + O$, with $v > w$

The reaction rate coefficient is then determined based on the following expression:

$$K(T, v, \Delta v) = DegF \cdot exp(a_1(v,\Delta v) + \frac{a_2(v,\Delta v)}{\ln(T)} + a_3(v,\Delta v) \cdot \ln(T) \quad (23)$$

where Δv is $(v - w)$

$$a_i(v,\Delta v) = b_{i1}(\Delta v) + b_{i2}(\Delta v) \cdot \ln(v) + \frac{b_{i3}(\Delta v) + b_{i4}(\Delta v)v + b_{i5}(\Delta v)v^2}{10^{21} + \exp(v)} \quad (24)$$

$$b_{ij}(\Delta v) = c_{ij1} + c_{ij2} \cdot \ln(\Delta v) + c_{ij3} \cdot \Delta v \cdot \exp(-\Delta v) + c_{ij4} \cdot \Delta v \cdot \Delta v \quad (25)$$

The coefficients c_{ijk} have been generated using a linear least squares method and are reported in[52] where the degenary factor (DegF) is also explained.

S7. Lumping vibrational levels in the 2D non-thermal plasma model

To limit the calculation time in the 2D non-thermal model, we consider a reduced chemistry set, in which the 24 vibrational levels of N_2 and the 15 vibrational levels of O_2 are each grouped together in one lumped vibrational level.[3] The lumping is achieved by summing the number density of all vibrational levels into the lumped level number density n_g:

$$n_g = \sum_{i=0}^{j} n_i \#(26)$$

In which n_i is the number density of the ith vibrational level (n_0 is considered the ground state number density) where j = 24 for N_2 and j = 15 for O_2.

The conservation equation in the non-thermal plasma model is then solved for the lumped level density n_g:

$$\frac{\partial n_g}{\partial t} + \nabla\left(D\nabla n_g\right) + \left(\vec{u_g}.\nabla\right)n_g = R_g \#(27)$$

In which D is the diffusion coefficient, $\vec{u_g}$ the gas flow velocity vector and R_g the sum of all production and loss rates R_i of each individual vibrational level due to chemical reactions:

$$R_g = \sum_{i=0}^{j} R_i \#(28)$$

After the calculation of n_g, the number density of each individual vibrational level within the group is described assuming a Maxwellian vibrational distribution function using the energy of the vibrational levels E_i and the vibrational temperature T_{vib}:

$$n_i = \frac{n_g exp\left(-\frac{E_i}{k_b.T_{vib}}\right)}{\sum_{i=0}^{j} exp\left(-\frac{E_i}{k_b.T_{vib}}\right)} \#(29)$$

In which k_b is the Boltzmann constant.

T_{vib} is calculated using the mean vibrational energy that is acquired by the N_2 and the O_2 molecules averaged over their vibrational levels. This mean vibrational energy $\bar{E_{vib}}$ is calculated through:

$$\frac{\partial n_g \bar{E_{vib}}}{\partial t} + \nabla.\left(D\nabla\left(n_g\bar{E_{vib}}\right)\right) + \left(\vec{u_g}.\nabla\right)n_g\bar{E_{vib}} = R_{E_{vib}} \#(30)$$

Where $R_{E_{vib}}$ is the sum of all vibrational energy production and loss rates due to chemical reactions in which vibrational energy is exchanged. These reactions are electron impact vibrational excitation, vibrational-translational (VT) relaxation and vibrational-vibrational (VV) relaxation.

T_{vib} is then calculated using the following relation between T_{vib} and $\bar{E_{vib}}$:

$$\bar{E_{vib}} = \frac{\sum_{i=0}^{j} E_i exp\left(-\frac{E_i}{k_b.T_{vib}}\right)}{\sum_{i=0}^{j} exp\left(-\frac{E_i}{k_b.T_{vib}}\right)} \#(31)$$

S8. Grouping of the particle trajectories

"For each of the 10 groups in figure 8 of the main paper, a quasi-1D simulation is performed, resulting in the calculated NO_x concentration in figure 9 of the main paper. Table S9 shows the temperature range of each group, the peak values of the average temperature and power density profiles that were used as input for these quasi-1D simulations, as well as the gas fraction in each group. These temperature and power density profiles were calculated by the (corrected) 3D thermal plasma model."

Table S9: *Average peak temperature and power density for each group of particles of figure 8 of the main paper (cf. temperature range in first column). The fraction of gas molecules in each group, as shown by the distribution in figure 8 of the main paper, is shown in the last column.*

Temperature range (K)	Average temperature (K)	Average power density (W/m3)	Gas fraction (%)
293-1000	613 ± 257	0	2.18
1000-1500	1280 ± 138	0	2.71
1500-2000	1733 ± 147	0	9.17
2000-2200	2097± 55	(4.3 ± 1.1) e7	5.40
2200-2400	2313± 58	(9.9 ± 2.1) e7	5.52
2400-2600	2502± 56	(1.90 ± 0.36) e8	7.36
2600-2800	2734± 48	(4.08 ± 0.61) e8	28.3
2800-3000	2872± 50	(6.31 ± 0.96) e8	34.3
3000-3200	3065± 56	(1.06 ± 0.14) e9	4.24
3200-3500	3266±52	(1.60 ± 0.15) e9	0.739

S9. Experimental setup

Figure S4 shows the experimental setup of our RGA plasma. The arc discharge is generated by a 10 kV DC power supply (Topower TN-XXZ02). A 25 kΩ ballast resistor is connected to the circuit to compensate for changes in the discharge current and to prevent over-heating of the plasma, allowing for a maximum current of 280 mA. The discharge voltage is measured by a high-voltage probe (TESTEC 1000:1), and the discharge current is determined from the voltage drop across a 25 Ω resistor. The time-resolved waveforms of the discharge voltage and current are recorded by an oscilloscope (Keysight DSOX1102A, 70 MHz bandwidth, 2GSa/s sample rate). The flow rates of the N_2 and O_2 feed gases (99.999% in purity) are controlled by mass flow controllers (Bronkhorst model F-201CV). The total flow rate is fixed at 2 L min^{-1}, and the gas feed ratio between N_2 and O_2 is varied from 20/80 to 80/20. The exhaust gas (comprising the product and unconverted feed gas) is analysed using a non-dispersive infra-red (NDIR) sensor, along with an ultra-violet sensor, for quantitative analysis of the species concentration (EMERSON Rosemount X-STREAM Enhanced XEGP continuous Gas Analyzer). The X-STREAM system is configured with four gases, two of which were used for this work: NO and NO_2. Exhaust gas from the RGA was input into the system at a flow rate of 500 mL/min through the use of a Bronkhorst mass flow controller; the specific flow rate of 500 mL/min was used as the system needed an input flow rate range between 50 mL/min and 1.5 L/min, although the choice of flow rate had no effect on the concentrations. The X-STREAM system was calibrated at the factory for NO_2 (UV sensor) and NO (NDIR sensor), and the calibration was again checked before measurements of the exhaust gas components, using known concentrations from 1% to 8%.

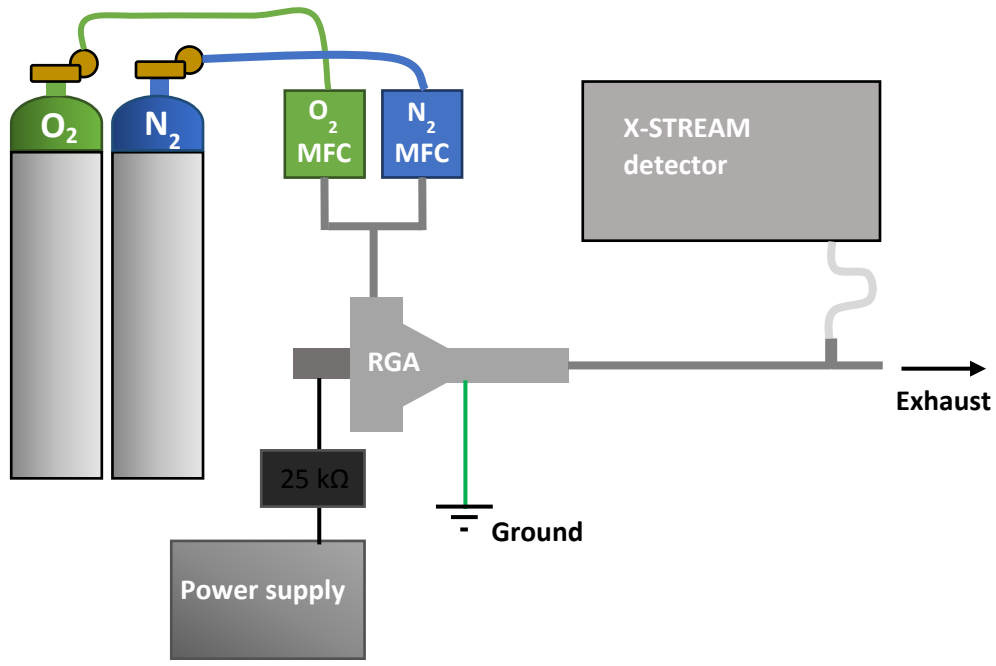

Figure S4: Experimental setup of the RGA reactor and X-STREAM detection device.

S10. Experimental yield relative to N_2/O_2 input

As many gas conversion applications report the process performance using the yield relative to the theoretical maximum, we also present this performance parameter using the following formula:

$$yield\ (\%) = \frac{achieved\ NO_x\ concentration}{theoretical\ maximum\ achievable\ NO_x\ concentration} \#(32)$$

This performance parameter offers additional insight in the plasma-based process, as it reports how efficient the resources of the N_2/O_2 input stream are used for NO_x production by comparing the achieved NO_x concentration to the maximum NO_x concentration that could be achieved within each gas mixture. However, for NO_x production, we need to treat this performance parameter with caution as the calculation of the theoretical maximum achievable NO_x concentration requires an assumption for the NO/NO_2 ratio. Indeed, this ratio determines heavily how much O_2 of the input stream is consumed for the NO_x production, given that there is twice as many O atoms in NO_2 as there are in NO. Since we don't know the NO/NO_2 ratio in an optimised plasma process, we can only report the yield if we assume that we currently achieved the optimal NO/NO_2 ratio. Using this assumption, we present the experimental yield relative to the N_2/O_2 input in figure S5. This figure shows a very similar trend as figure 15 of the main paper, having a maximum around the 50/50 N_2/O_2 input mixture, but also shows an even greater maximum at the 20/80 N_2/O_2 mixture. Indeed, due to the low amount of N_2 (20%) in the input gas stream of this mixture, a low theoretical maximum achievable NO_x (47.66 %) concentration is expected. As the NO_x concentration in this mixture (2.68 %) is not so low compared to the other mixtures (see figure 15 of the main article), the achieved yield in this mixture is high, indicating that this mixture uses the input resources of the N_2/O_2 input stream most efficiently.

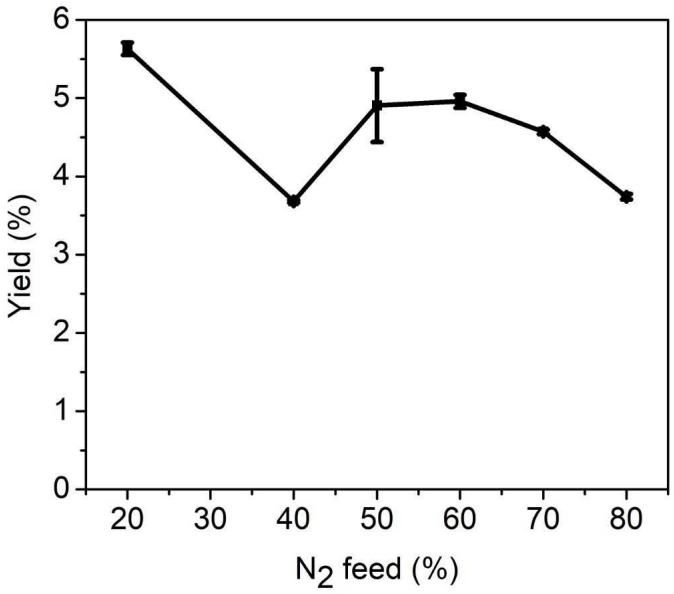

Figure S5: Experimental yield relative to the N_2/O_2 input at different N_2 feed ratios at an applied power of 106 W and flow rate of 2 L min^{-1}, calculated using equation 32.

References

(1) Menter, F. R.; Kuntz, M.; Langtry, R. Ten Years of Industrial Experience with the SST Turbulence Model. *Turbul. Heat Mass Transf.* **2003**, *4*, 625–632.

(2) COMSOL Multiphysics® v. 5.5. Www.Comsol.Com. COMSOL AB, Stockholm, Sweden.

(3) Berthelot, A.; Bogaerts, A. Modeling of Plasma-Based CO2 Conversion: Lumping of the Vibrational Levels. *Plasma Sources Sci. Technol.* **2016**, *25*, 045022.

(4) Vervloessem, E.; Aghaei, M.; F., J.; Hafezkhiabani, N.; Bogaerts, A. Plasma-Based N2 Fixation into NOx : Insights from Modelling toward Optimum Yields and Energy Costs in a Gliding Arc Plasmatron. *ACS Sustain. Chem. Eng*.

(5) Laporta, V.; Little, D. A.; Celiberto, R.; Tennyson, J. Electron-Impact Resonant Vibrational Excitation and Dissociation Processes Involving Vibrationally Excited N2molecules. *Plasma Sources Sci. Technol.* **2014**, *23*, 065002.

(6) Alves, L. L. E + N2 => N2^+ + 2e Exc to B3PG C3PU A3Suv4 A1Su and N(Ex). *J. phys. Conf. Ser.* **2014**, *656*, 1.

(7) Morgan database, www.lxcat.net, retrieved in february 2018.

(8) Alves, L. L. The IST-Lisbon Database on LXCat. *J. phys. Conf. Ser.* **2014**, *565*.

(9) Phelps Database, www.lxcat.net, Phelps, A.V.; Pitchford, L. C. Anisotropic Scattering of Electrons by N2 and Its Effect on Electron Transport. *Phys. Rev.* **1985**, *31*, 2932.

(10) Tennyson, V.; Laporta, R. . C. J. O2 Vibrational Excitation CS. *plasma sources sci. Technol.* **2013**, *22*, 025001.

(11) Itikawa, Y. Cross Sections for Electron Collisions with Oxygen Molecules. *J. Phys. Chem. Ref. Data* **2009**, *38*, 1–20.

(12) Eliasson, B.; Kogelschatz, U. *Basic Data for Modelling of Electrical Discharges in*

Gases: Oxygen; Baden: ABB Asea Brown Boveri, 1986.

(13) IST-Lisbon database, www.lxcat.net, retrieved in february 2018.

(14) Lawton, S. A.; Phelps, A. V. Excitation of the b^1 sigma_g^+ state of O_2 by low energy electrons.

(15) Khvorostovskaya, L. E.; Yankovsky, V. A. Negative Ions, Ozone, and Metastable Components in Dc Oxygen Glow Discharge. *Contrib. to Plasma Phys.* **1991**, *31*, 71–88.

(16) Hokazono, H.; Obara, M.; Midorikawa, K.; Tashiro, H. Theoretical Operational Life Study of the Closed-Cycle Transversely Excited Atmospheric CO2laser. *J. Appl. Phys.* **1991**, *69*, 6850–6868.

(17) Itikawa database, www.lxcat.net, retrieved in february 2018.

(18) Quantemol database, www.lxcat.net, retrieved in february 2018.

(19) Hayashi database, www.lxcat.net, retrieved in february 2018.

(20) Gordillo-V'azquez, F. J. Air Plasma Kinetics under the Influence of Sprites. *J. Phys. D. Appl. Phys.* **2008**, *41*, 234016.

(21) Wang, W.; Snoeckx, R.; Zhang, X.; Cha, M. S.; Bogaerts, A. Modeling Plasma-Based CO2 and CH4 Conversion in Mixtures with N2, O2, and H2O: The Bigger Plasma Chemistry Picture. *J. Phys. Chem. C* **2018**, *122*, 8704–8723.

(22) Capitelli, M.; Ferreira, C. M.; Gordiets, B. F.; Osipov, A. I. *Plasma Kinetics in Atmospheric Gases*; 2000.

(23) Kewley, D. J.; Hornung, H. G. Free-Piston Shock-Tube Study of Nitrogen Dissociation. *Chem. Phys. Lett.* **1974**, *25*, 531–536.

(24) Clyne, M. A. A. .; Stedman, D. H. Rate of Recombination of Nitrogen Atoms. *J. Phys. Chem.* **1967**, *71*, 3071–3073.

(25) Van Gaens, W.; Bogaerts, A. Erratum: Kinetic Modelling for an Atmospheric Pressure

Argon Plasma Jet in Humid Air (J. Phys. D: Appl. Phys. 46 (2013) 275201)). *J. Phys. D. Appl. Phys.* **2014**, *47*.

(26) Tsang, W.; Hampson, R. F. Chemical Kinetic Data Base for Combustion Chemistry. Part I. Methane and Related Compounds. *J. Phys. Chem. Ref. Data* **1986**, *15*, 1087–1279.

(27) Atkinson, R.; Baulch, D. L.; Cox, R. A.; Hampson, R. F.; Kerr Chairman, J. A.; Troe, J. Evaluated Kinetic and Photochemical Data for Atmospheric Chemistry: Supplement III. IUPAC Subcommittee on Gas Kinetic Data Evaluation for Atmospheric Chemistry. *J. Phys. Chem. Ref. Data* **1997**, *18*, 881–1097.

(28) Hippler, H.; Rahn, R.; Troe, J. Temperature and Pressure Dependence of Ozone Formation Rates in the Range 1-1000 Bar and 90-370 K. *J. Chem. Phys.* **1990**, *93*, 6560–6569.

(29) Heimerl, J. M.; Coffee, T. P. The Unimolecular Ozone Decomposition Reaction. *Combust. Flame* **1979**, *35*, 117–123.

(30) Suzzi Valli, G.; Orrú, R.; Clementi, E.; Laganà, A.; Crocchianti, S. Rate Coefficients for the N+O2reaction Computed on an Ab Initio Potential Energy Surface. *J. Chem. Phys.* **1995**, *102*, 2825–2832.

(31) Baulch, D.L.; Cobos, C.J.; Cox, R.A.; Frank, P.; Hayman, G.; Just, Th.; Kerr, J.A.; Murrells, T.; Pilling, M.J.; Troe, J.; Walker, R.W.; Warnatz, J. Evaluated Kinetic Data for Combusion Modelling. Supplement I. *J. Phys. Chem. Ref. Data* **1994**, *23*, 847–1033.

(32) Hjorth, J. No Title. *Int. J. Chem. Kinet.* **1992**, *24*, 51–65.

(33) Herron, J. T. Rate of the Reaction NO+N. *J. Chem. Phys.* **1961**, *35*, 1138–1139.

(34) Bemand, P. P.; Clyne, M. A. A.; Watson, R. T. Atomic Resonance Fluorescence and Mass Spectrometry for Measurements of the Rate Constants for Elementary Reactions:

O 3PJ + NO 2 → NO + O2 and NO + O3 → NO 2 + O2. *J. Chem. Soc. Faraday Trans. 2 Mol. Chem. Phys.* **1974**, *70*, 564–576.

(35) Atkinson, R.; Baulch, D. L.; Cox, R. A.; Crowley, J. N.; Hampson, R. F.; Hynes, R. G.; Jenkin, M. E.; Rossi, M. J.; Troe, J.; Center, P. R.; et al. Evaluated Kinetic and Photochemical Data for Atmospheric Chemistry: Volume I – Gas Phase Reactions of O. *J. Phys. Chem. Ref. Data* **2004**, *I*, 1461–1738.

(36) No, I. R. I.; Tsang, W.; Herron, J. T. Chemical Kinetic Data Base for Propellant Combustion. **1991**, *20*.

(37) Graham, R.A.; Johnston, H. S. The Photochemistry of NO3 and the Kinetics of the N2O5-O3 System. *J. Phys. Chem.* **1978**, *82*.

(38) Ashmore, P.G.; Burnett, M. G. Concurrent Molecular and Free Radical Mechanisms in the Thermal Decomposition of Nitrogen Dioxide. *J. Chem. Soc. Faraday Trans. 2* **1962**.

(39) Campbell, I. M.; Thrush, B. A. Behaviour of Carbon Dioxide and Nitrous Oxide in Active Nitrogen. *Trans. Faraday Soc.* **1966**, *62*, 3366–3374.

(40) Nighan, W. L. Electron Rates Excited. **1970**, *2*.

(41) Kossyi, I. A.; Kostinsky, A. Y.; Matveyev, A. A.; Silakov, V. P. Kinetic Scheme of the Non-Equilibrium Discharge in Nitrogen-Oxygen Mixtures. *Plasma Sources Sci. Technol.* **1992**, *1*, 207–220.

(42) Beverly, R. E. Ion Aging Effects on the Dissociative-Attachment Instability in CO2 Lasers. *Opt. Quantum Electron.* **1982**, *14*, 501–513.

(43) Whitaker, M.; Biondi, M.A.; Johnsen, R. Electron-Temperature Dependence of Dissociative Recomination of Electrons with N2^+. *Phys. Rev. A* **1981**, *24*, 743–745.

(44) Gudmundsson, J. T.; Thorsteinsson, E. G. Oxygen Discharges Diluted with Argon: Dissociation Processes. *Plasma Sources Sci. Technol.* **2007**, *16*, 399–412.

(45) Ionin, A. A.; Kochetov, I. V.; Napartovich, A. P.; Yuryshev, N. N. Physics and Engineering of Singlet Delta Oxygen Production in Low-Temperature Plasma. *J. Phys. D. Appl. Phys.* **2007**, *40*.

(46) Cenian, A.; Chernukho, A.; Borodin, V. Modeling of Plasma-Chemical Reactions in Gas Mixture of CO2 Lasers. II. Theoretical Model and Its Verification. *Contrib. to Plasma Phys.* **1995**, *35*, 273–296.

(47) Beuthe, T. G.; Chang, J.-S. Related Content Chemical Kinetic Modelling of Non-Equilibrium Ar- CO 2 Thermal Plasmas. *Jpn. J. Appl. Phys.* **1997**, *36*, 4997–5002.

(48) Eliasson, B.; Hirth, M.; Kogelschatz, U. Ozone Synthesis from Oxygen in Dielectric Barrier Discharges. *J. Phys. D. Appl. Phys.* **1987**, *20*, 1421–1437.

(49) Mcfarland, M.; Dunkin, D. B.; Fehsenfeld, F. C.; Schmeltekopf, A. L.; Ferguson, E. E. Collisional Detachment Studies of NO-. *J. Chem. Phys.* **1972**, *56*, 2358–2364.

(50) Adamovich, I. V.; MacHeret, S. O.; Rich, J. W.; Treanor, C. E. Vibrational Energy Transfer Rates Using a Forced Harmonic Oscillator Model. *J. Thermophys. Heat Transf.* **2008**, *12*, 57–65.

(51) Esposito, F.; Armenise, I.; Capitelli, M. N-N2 State to State Vibrational-Relaxation and Dissociation Rates Based on Quasiclassical Calculations. *Chem. Phys.* **2006**, *331*, 1–8.

(52) Esposito, F.; Armenise, I.; Capitta, G.; Capitelli, M. O-O2 State-to-State Vibrational Relaxation and Dissociation Rates Based on Quasiclassical Calculations. *Chem. Phys.* **2008**, *351*, 91–98.